Dr. P. George Huang
Professor and Chair
Department of Mechanical and Materials Engineering
Wright State University
Dayton, OH 45435
Ph: +1 937 775 5043; Email: George.huang@wright.edu

THINkS: A Novel Tool for Multiscale CFD Calculations of Human Blood Circulation

Abstract

Computational Fluid Dynamics (CFD) is emerging as a tool for better assessment and management of cerebral aneurysms. CFD calculations are often restricted to a small arterial zone and the solution is sensitive to boundary conditions prescribed. A 1D simulation of the complete vessel network, THINkS (Total Human Intravascular NetworK Simulation), is introduced to better describe the boundary conditions and to provide an overall flow information of the complex vessel network.

As the governing equations for the blood flow in human vessel system can be casted in the same form as the gas dynamic equations, the traditional shock capturing scheme can be modified to solve the hemodynamic equations. In this talk we will discuss an in-house computer program - THINkS. THINkS consists of a simulation of 85 major arteries, 158 major veins, 43 arterial and 77 venous junctions. Blood flow in arterioles, capillaries and venules is modeled using lumped parameter models, or the 0D models, which are modeled using the connection of a number of capacitors, resistors and inductors to represent the real physics. The model used a simple 0D model for 20 one-artery-to-one-vein micro circulations and 4 other 0D models for 7 complex arteries-to-veins micro circulations. Moreover, a 4-chamber 0D model for the heart is used to allow blood to pump from superior vena cava I and inferior vena cava I veins, through the pulmonary system, and discharge back to the ascending aorta artery. In addition to the 4 valves inside the heart, there are also 15 venous valves used in the venous system.

THINkS calculations indicated usefulness of the model in predicting the trends of cerebral flow patterns. THINkS solutions were validated with a number of in vivo experimental data and the agreement was excellent. A comparison with experiments for the impact of incomplete circle of Willis (CoW) to the flow patterns was also made and the trend shows an excellent agreement with reported data. THINkS allows for more accurate boundary conditions for 3D zonal-based CFD calculations. THINkS has been validated against available experimental data and shown to respond correctly to the flow pattern change caused by the variation in CoW. It provides the detailed flow information of the entire human body including cerebral vessel network. Our aim is to use THINkS to generate accurate flow assessments, guide treatment plans, and more reliably predict risks associated with vascular lesions.

Available online at www.sciencedirect.com

ScienceDirect

Procedia Engineering 00 (2015) 000–000

Procedia Engineering

www.elsevier.com/locate/procedia

6th BSME International Conference on Thermal Engineering (ICTE 2014)

Measurement and Observation of Elementary Transition Boiling Process after Sudden Contact of Liquid with Hot Surface

Yuichi MITSUTAKE[a,*] , Suhaimi ILLIAS[b], Koutarou TSUBAKI[b], Mohammad Nasim Hasan[c], Masanori MONDE[d]

[a]*Institute of Ocean Energy, Saga University, 1 Honjo-machi, Saga-shi, Saga Japan*
[b]*Department of Mechanical Engineering, Saga University, 1 Honjo-machi, Saga-shi, Saga Japan*
[c]*Department of Mechanical Engineering, Bangladesh University of Engineering & Technology, Dhaka-1000, Bangladesh*
[d]*Reserch Cemeter for Hydrogen Industrial Use and Storagey,Kyusyu University, 744 Motooka,Nishi-ku, Fukuoka-shi, Fukuoka Japan*

Abstract

A Fast response surface temperature measurement technique has been developed to investigate transient transition boiling phenomena after ethanol droplet impact on a nickel hot surface. Our motivation is to make clear the mechanism of boiling transition between nucleate and film boiling which is closely related the recovery of wetting on the hot surface being higher than the Leidenfrost temperature. In this study transient boiling phenomena during sudden contact of an ethanol sessile droplet on a hot solid surface has been investigated to understand what governs whether the solid surface keeps wet or not. The droplet impact boiling system is very simple and easier to observe but it includes the elementary transition boiling process. Since the transient transition took place within a couple ten milliseconds, observation with high speed video system and fast response surface temperature measurement technique are essential for better understanding of the transition boiling phenomena.

The experiments were conducted for single and multiple droplet impacts. The multiple droplet impacts simulates liquid and solid contact situations on a hot surface during spray or laminar jet quench. The nickel disk of 50 mm in diameter and 5 mm in thickness was used as the hot surface. The hot surface was inclined from 0 deg (horizontal) to 40 deg. The fast-response film thermocouple with a typical minimum response time of 80 microseconds was developed and fabricated on the nickel disk at the depth of 3 micrometers from the surface. The temperature histories just beneath the surface were recorded at the sampling frequency of 200 kHz. The boiling phenomena beneath a sessile droplet impacted on the hot surface were observed by using a microscope equipped with the high speed video camera at the maximum frame rate of 22.5 kfps. The surface temperature and surface heat flux were estimated with 1D inverse heat conduction analysis. Histories of local surface temperature and local heat flux were compared with the boiling video image. The experiments were done for different initial wall temperatures up to 250 ^{o}C, different liquid subcoolings from 33 to 53 K. The multiple impact frequency was changed from 280 to 840 Hz.

* Corresponding author. Tel.: +81-952-28-8616; fax: +81-952-28-8587.
E-mail address: mitutake@me.saga-u.ac.jp

Peer-review under responsibility of organizing committee of the 6th BSME International Conference on Thermal Engineering (ICTE 2014).

In case of the single droplet impact tests, the observation results showed that wetting situation was maintained for very short time even though the surface temperature was beyond the liquid superheat limit temperature. We defined the vapor film generation time as the characteristic boiling transition time scale from wetted nucleation boiling regime to dry film boiling regime. The film generation time were measured for the extensive initial surface temperature range, different subcoolings and different impact velocities. As the initial surface temperature increased, the film generation time decreased to order of microsecond and film boiling situation seemed to be established via spontaneous nucleation (vapor explosion) process. In case of the multiple droplets impact tests, film generation times were evaluated every droplet impact during continuous cooling from the initial solid temperature. As long as the generation time was less than 1 millisecond and much shorter than the impact period, stable film boiling was observed. Then the film generation time increased with the droplet impact times and approached to the droplet impact period as the cooling time elapsed. This region was recognized as the transition boiling region. After the generation time reached to the droplet impact period and then stable wetted situation, namely nucleate boiling was observed. As compared with the single impact tests, the generation time for the multiple impact became shorter than that for the single droplet impact at same initial surface temperature and the lower limit surface temperature observed vapor film generation was reduced. This fact may imply the effect of transient heat conduction on the wetting temperature shifts to higher wall superheat temperature beyond liquid superheat limit temperature during quenching with jets or sprays.

Peer-review under responsibility of organizing committee of the 6th BSME International Conference on Thermal Engineering (ICTE 2014).

Keywords: Fast-response temperature measurement; Transient transition boiling; Droplet; Wetting phenomenon

1. Introduction

In the fields of material manufacturing, dip, laminar jet and spray quenches are commonly used as heat treatment of materials to improve mechanical strength. Recent material production processes such as hot strip rolling require more accurate cooling temperature control and more uniform temperature distribution of the surface during jet or spray quenching. Because most of target cooling temperatures range in unstable transition boiling regime, precise temperature control of the materials becomes difficult to product high value added materials or improve mechanical properties of materials.

The transition boiling regime indicates negative gradient on boiling curve and it shows an inherent unsteady nature due to strong coupling phenomena of boiling heat transfer with transient heat conduction in the solid wall. It is known that boiling transition from film boiling to nucleate boiling is closely related with recovery of wetting situation on the hot surface and the transition boiling regime is characterized with coexisting of partial wet (nucleate boiling) and dry (film boiling) situation. When stable wetted situation is recovered, heat transfer coefficient of the nucleate boiling increases one or two digits as compared with that of the film boiling regime. Therefore, accurate prediction of surface wetting at the inception transition boiling is required for the precise cooling temperature controls. Recovery of the wetting situation on the hot surface is commonly recognized as the minimum heat flux (MHF) point on the boiling curve. However, our knowledge about the transition boiling heat transfer region is not enough to predict and control quenching processes in despite of a lot of studies over about 80 years after the first discovery of the boiling curve by Nukiyama [1]. Because the wetting phenomenon and the transition boiling heat transfer have unsteady nature due to strong coupling of the transient heat conduction in the solid wall with the boiling heat transfer on the surface. Deeper understanding about the elementary processes of the wetting phenomenon is required. However, wetting phenomena takes place so fast during quenching, the existing direct temperature measurement techniques are not enough to understand the elementary transient boiling process in detail.

In this study we focused on evaluation and observation of transient boiling heat transfer accompanied wetting phenomena beneath a sessile liquid layer formed by impact of a droplet on a hot surface. The droplet impact tests on the surface make observations of transition boiling heat transfer region easier due to simple liquid and vapor flow situations as compared with the other boiling systems like pool and external flow boiling systems. There are many existing studies on heat transfer with fast response surface temperature measurement techniques [2-12]. The fast response measurement techniques are categorized into three types, Category-1: flash mounted very thin sheath thermocouple [2, 3], Category-2: overlapped micro thin deposited film thermocouple on an electrically insulated

substrate with spattering, plating or MEMS processes [4, 5], and Category-3: deposited thin film and wire junction on the surface [6-12]. As the significant studies, Groendes and Mesler [2] performed water drop experiments on a hot surface being higher than Leidenfrost temperature and measured period of transient liquid-solid contact from wall thermocouple signal. Nakabeppu and Wakasugi [5] measured distribution of surface heat flux due to evaporation on microlayer beneath bubbles with the overlapped micro Ni-Chromel film thermocouples on silicon substrate. They reported maximum response frequency of the thermocouples was 10 kHz. However, the category-2 technique is difficult to apply to measurement of transient transition boiling on a thick metal surface. Because excess thermal stress and high temperature operation damage the sensor. Most of studies introduced above were limited to the applications to nucleate pool boiling. As the earliest study of the transient boiling measurement technique with the category-3 type thermocouple, Moore and Mesler[6] made a K-type hot junction just beneath the nichrome heater surface by plating a nickel layer of 1.3 μm on it. They measured transient surface temperature change corresponding to evaporation and dryout of micro liquid layer during pool boiling at high heat flux region. In this study there was no choice other than the category-3 thermocouple to realize transient boiling on a thick metal surface which can operate at very high temperature and keep intact condition of the hot junctions against surface oxidization, thermal stress due to impacts of droplet. We tried to fabricate fast response thermocouples which can detect local temperature fluctuations over 10 kHz on a hot surface. Local surface temperature and surface heat flux were evaluated with a revised inverse heat conduction analysis proposed by the authors [13, 14].

The droplet impact tests were conducted with the single droplet and the multiple droplets. Generally liquid and solid contacts during spray or laminar jet quenching are autonomously controlled by hydrodynamic of two phase flow boiling and irregular liquid and solid contact situations become very difficult to evaluate. Thus observations of transient boiling with the multiple droplet impacts may provide transient transition boiling situation from the film boiling to nucleate boiling under control the frequency of the liquid and solid contacts. The difference between the single and multiple droplet impacts is just difference in the initial solid temperature distributions. In case of the single droplet, the transient boiling started from the uniform initial solid temperature. But the initial temperature distribution in the solid was affected by the past transient heat conduction due to the previous droplet impacts. The effect of the previous impacts will be disappear as impact frequency becomes smaller. In this study we measured and observed the transient transition boiling during the single and multiple droplet impacts in detail with fast response surface temperature measurement technique and high speed video over extensive ranges of the initial surface temperature, degree of liquid subcooling, inclined angle of the surface and droplet impact velocity.

Nomenclature

a	thermal diffusivity (m^2/s)
c	specific heat (J/kg/K)
f	frequency (Hz)
k	thermal conductivity (W/m/K)
q	heat flux (W/m^2)
t	time (s)
u	droplet impact velocity (m/s)
x	space coordinate perpendicular to surface (m)
N	maximum order of approximate half polynomial function
T	temperature (^oC)
Greek letters	
β	ratio of thermal inertia of solid and liquid = $\sqrt{(\rho_s c_s k_s)/(\rho_l c_l k_l)}$, -
δ	thickness of nickel deposit layer (m)
λ	wave length (m)
ρ	density (kg/m^3)
Δt	data sampling period (s)
ΔT_{sat}	degree of wall superheat (K)
ΔT_{sub}	degree of liquid subcooling (K)

Subscripts	
0	initial / reference
break	liquid film break
c	cut off
cr	critical
film	vapour film generation
i	liquid and solid interface
j	hot junction at $x = \delta$ or jet
l	liquid phase
LF	lower limit of vapour film generation
n	nozzle
s	solid phase
SHL	liquid superheat limit
w	wall

2. Experimental setup and procedure

2.1. Thin film-wire thermocouple

Figures 1 and 2 show a structure of category-3 film-wire thermocouple, and photographs of a disk and a hot junction. A nickel disk of 50 mm in diameter and 5 mm in thickness was used for heated surface. As shown in Fig.2(a), nine throughholes were formed on the central portion of the disk (denoted with the red circle) with electric discharge machining (EDM) and those were arranged square lattice at the pitch of 2.5 mm. Electrically insulated chromel wire with SiO_2 coat was fixed in a hole and the top surface was polished until the tips of the wires became flush with the nickel surface as shown in Fig.2(b). Averaged surface roughness R_a along the center line of the disk was indicated as 0.449 μm. Since outer surface of a wire was insulated from the nickel disk, the contact area of the nickel deposit layer and the tips of the chromel wires were served as Chromel-Nickel hot junctions just below the nickel disk surface. Combination of Chromel (70%Ni-30%Cr alloy) and Nickel was selected due to large Seebeck coefficients and oxidation resistance of nickel under high temperature operation up to 300 °C.

A response time of thin film-wire thermocouple strongly depends on the thermal properties of the materials and depth of the junction. In order to make the thermocouple design better, temperature response at a hot junction is evaluated by using one-dimensional transient heat conduction analysis. The thickness of the nickel deposit layer δ and thermal diffusivity a_s of the film on the time response were evaluated by using an exact solution of one dimensional semi-infinite solid and the thickness of a nickel layer was decided. When a harmonic surface temperature fluctuation propagates into a solid, the temperature oscillation is diminished as going into the solid deeply. The attenuation of the harmonic wave amplitude is given by Eq.(1) [15].

$$e^{-2\pi \cdot x/\sqrt{4\pi a_s / f}} = e^{-2\pi \cdot x/\lambda} \tag{1}$$

Here, f is a frequency of the harmonic wave, a_s is a thermal diffusivity of the solid and λ is a wave length. The decay factor becomes very small value ($e^{-2\pi} = 0.0019$) at the depth of a wave length $\lambda = (4\pi a_s / f)^{1/2}$. Supposing the decay factor as 1/2 for present hot junction, it can be derived the critical depth δ_{cr} as Eq.(2) for certain frequency and film material.

$$\delta_{cr} = 0.195\sqrt{a_s / f} \tag{2}$$

In case of thermal diffusivity of nickel a_s = 23.9 mm^2/s and f = 100 kHz, the critical thickness δ_{cr} of 6 μm will be evaluated with Eq.(2). Thus the nickel layer of 3 μm was deposited on the disk with electroless nickel plating process. As shown in Fig.1 chromel wires and the nickel disk were welded to the chromel and nickel wires and connected to the cold junctions in the ice box. The thermal electromotive forces were amplified with the D.C.

isolation amplifiers (maximum gain of 1000, frequency band from D.C. to 2 MHz), and sampled and recorded with a high speed analog input device card installed in a PC (12 bit A/D converter, four channels simultaneous sampling at the maximum frequency of 10 MHz).

Relationship between temperature and thermal electromotive force of each hot junction was calibrated from room temperature to 280 ^{o}C before use. Typical thermopower of a chromel-nickel junction was 41.9 μV/K.

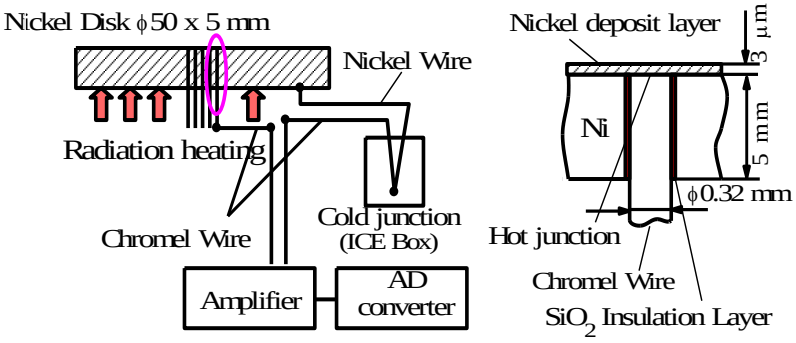

Fig.1 film-wire fast response thermocouple

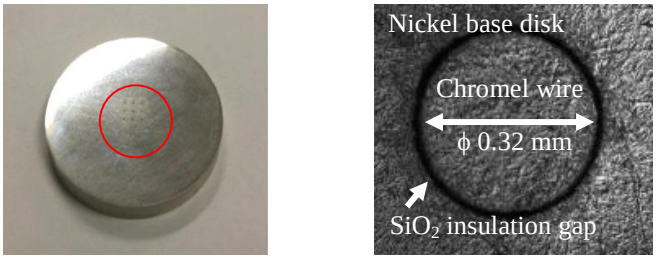

Fig.2 Photographs of heated disk and assemble of thermocouple. (a) Nickel base disk (thickness 5 mm, diameter ϕ50 mm), (b) Close-up of hot junction area (before Ni plating)

2.2. Inverse heat conduction analysis technique

Since the thermal penetration depth from the surface with transient heat conduction in the solid is proportional to $(a_s t)^{1/2}$, the penetration depth for nickel after 1 ms is the order of 0.1 mm. As discussed later, typical liquid-solid contact time was a few milliseconds. Therefore, it can be assumed the Ni disk of 5 mm thickness as a semi-infinite solid. Hot junctions were formed at the depth of 3 μm from the surface. The measured temperature may be treated as the surface temperature. However, a one dimensional inverse heat conduction analysis for semi-infinite homogeneous isotropic solid was applied to estimate local surface temperature and surface heat flux. The analytical technique was originally given by Monde [13] and improved by Woodfields, et al. [14].

The inverse analysis solved the governing equation given in Eq.(3) with the initial and boundary conditions given in Eqs.(4) and (5) was analytically solved in complex space after the Laplace transformation. In contrast with the well-known conjugated gradient techniques, the sampled transient temperature history at the internal single location $x = \delta$ was approximated with a half-polynomial power series function as Eq.(6) to solve Eq.(3) with the analytical procedure. In Eq.(6) the integer N is the maximum order of the half-polynomial, t_0 is the reference time, the coefficients of b_i are decided by least square method and sample data, and Γ is the gamma function. For reference, thermal properties of the materials: nickel, chromel, ethanol and silicon dioxide (Insulator) are tabulated in Table 1 [16].

$$\frac{\partial T}{\partial t} = a\frac{\partial^2 T}{\partial x^2} \qquad x \geq 0,\ t > 0 \tag{3}$$

$$T = 0 \qquad x \geq 0,\ t = 0 \tag{4}$$

$$T(x,t) = f(t) \qquad x = \delta,\ t > 0 \tag{5}$$

$$f(t) = \sum_{i=0}^{N} b_i \cdot (t - t_0)^{i/2} / \Gamma((i/2)+1) \tag{6}$$

After long manipulation, finally the inverse solution of the temperature distribution in the solid was obtained as Eq.(7). Substituting x = 0 into Eq.(7) and the gradient of Eq.(7), we can get the surface temperature T_w and the surface heat flux q_w as given in Eqs.(8) and (9). The factor of P_i which is function of the space position x, the thermal diffusivity of the solid a and the temperature measuring position δ, is given as Eq.(10).

$$T(t,x) = \sum_{i=-1}^{\mathrm{int}((N+1)/2)} P_i(x.a,\delta) \cdot (t - t_0)^{\frac{i}{2}} / \Gamma(i/2+1) \tag{7}$$

$$T_w(t) = T(0,t) = \sum_{i=-1}^{\mathrm{int}((N+1)/2)} P_i(0,a,\delta) \cdot (t - t_0)^{i/2} / \Gamma(i/2+1) \tag{8}$$

$$q_w(t) = -k_s \left.\frac{\partial T}{\partial x}\right|_{x=0} = -k_s \cdot \sum_{i=-1}^{\mathrm{int}((N+1)/2)} \left.\frac{\partial P_i(x,a,\delta)}{\partial x}\right|_{x=0} (t - t_0)^{i/2} / \Gamma(i/2+1) \tag{9}$$

$$P_i(x,a,\delta) = \sum_{k=i}^{N} \sum_{m=0}^{N-i} \frac{b_k ((\delta - x)/a)^m}{m!}\ ,\ i \neq -1 \qquad P_{-1}(x,a,\delta) = \sum_{k=0}^{N-1} \sum_{m=1}^{N} \frac{b_k ((\delta - x)/a)^m}{m!}\ ,\ i = -1 \tag{10}$$

Table 1 Thermal diffusivity and thermal conductivity for materials at 300 K [16]

	Thermal diffusivity a , mm^2/s	Thermal conductivity k , W/m/K	Thermal inertia $(\rho ck)^{1/2}$, kJ/(m^{2}Ks$^{1/2}$)
Nickel	23.9	69.8	14.28
Chromel	3.9	13.8	6.99
Silicon dioxide (Insulator)	0.81	1.62	1.80
Ethanol	0.086	0.166	0.566

2.3. Ethanol droplet impact facilities

Schematics of experimental setups for single droplet impact tests and multiple droplet impacts tests can be seen in Figs. 3(a) and (b), respectively. The experimental apparatus consists of four systems, heated surface, optical observation and recoding system, droplet supply system and data acquisition system.

The heated surface was mounted on the top of the heater casing. A K-type thermocouple welded on the surface was used as reference temperature to control the radiation heater power. To prevent a rebounded droplet from colliding with the other droplets, the heated surface was slanted 30 degree from the vertical direction for the multiple droplet impacts test as shown in Fig.3. The optical observation was carried out by the stereo microscope equipped with a coaxial epi-illumination system (100 W) and a plan apochromat objective lens with a long working distance and the additional metal halide lamps (250W+350W) with fiber light guides. Transient boiling situation on the heated surface was recorded with the digital high speed camera connected to the trinocular tube of the microscope. A typical frame rate was 22,500 fps for the single droplet impact tests and 10,000 fps for the multiple droplet impacts at the fixed resolution of 640 x 480 pixels.

As shown in Figs.3 (a) and (b), the experimental systems except for the droplet supply system were common for the both tests. In the single droplet tests, the droplet dispenser like a stalagmometer, was used. A geared D.C. motor

driven micrometer syringe supplied test liquid to the vertical glass dispenser nozzle of 4 mm in outer diameter and 1.5 mm in inner diameter. A droplet was suspended below the bottom end surface of the nozzle until the gravity force increased beyond the force of surface tension, and it finally dropped off. Impact velocities of droplets were adjusted with the vertical height of the dispenser. For multiple droplet impacts tests, a series of droplets was generated by fragmentation of column liquid jet injected from the nozzle pipe of 1.5 mm in the inner diameter and 0.05 mm in the thickness due to the Rayleigh instability. To enhance and stabilize the fragmentation, the nozzle pipe was forcibly vibrated with the moving coil driven by the function generator. The vibration frequency f was decided with the Rayleigh instability wave length λ_R (= 4.508xd_j) and the injected velocity at the exit of the nozzle u_j. Ethanol was supplied from the liquid tank λ_R to the nozzle via the solenoid valve. u_j was adjusted by the air pressure in the liquid tank. In case of u_j = 3 m/s and diameter of the liquid column d_j = 1.5 mm, the basic harmonic frequency of the Rayleigh instability $f = u_j / \lambda_R$ corresponds to 280 Hz. In the present study, first, second and third orders of harmonics; 280, 560 and 840 Hz were tested. Impact velocities and diameters of droplets were measured with the side view high speed video camera at frame rates of 1,000 fps. Recording of the high speed video camera and the temperature measurement system were triggered with a TTL output signal transmitted from the photo interrupter synchronized with an initial falling droplet.

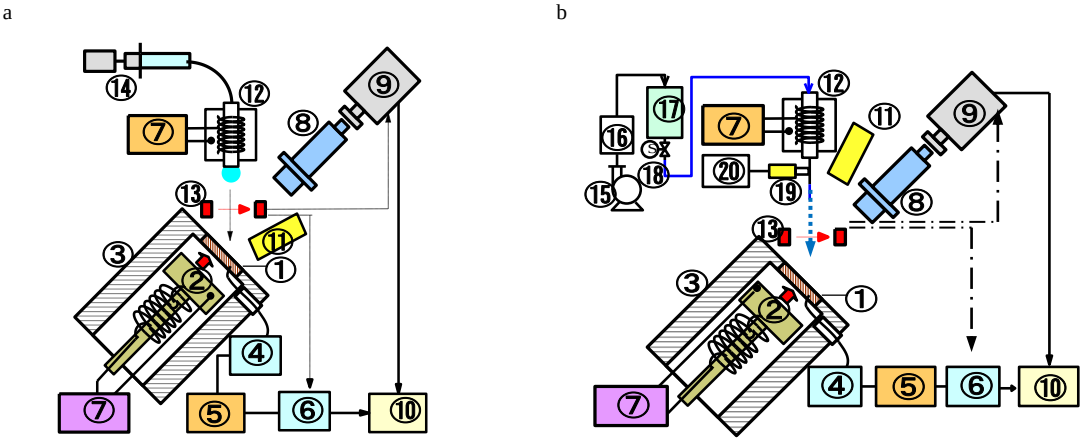

1.Nickel disk equipped with film-wire thermocouples 2.Radiation heater 3.Heater casing 4.Ice box 5.Isolation amplifier 6.A/D converter 7.Thermostat 8.Stereo microscope 9.High speed video camera 10.PC 11.Metal halide light source 12.Droplet dispenser 13. Photo interrupter 14.Micrometer syringe driven with geared motor 15.Air compressor 16.Pressure regulator 17.Liquid tank 18.Solenoid valve 19.Moving coil 20.Function generator

Figure 3 Schematic and photograph of experimental setup. (a) single droplet impact test facility; (b) multiple droplet impacts test facility

2.4. Experimental procedure

The Nickel disk was preheated at a designated initial temperature with the radiation heater. Initial temperature range included above and below 197 ^{o}C which is the superheat limit temperature of ethanol T_{SHL} (corresponding to spontaneous nucleation temperature) evaluated with the Lienhard's correlation [17]. A height of the droplet dispenser over the surface was adjusted for an impact velocity of a droplet. Location of the dispenser on a horizontal plane was carefully adjusted with a XY axis positioning stage to match the first contact point of a droplet with a hot junction on the heated surface. The droplet liquid was controlled at a designated temperature with the dispenser heater and the thermostat.

In single droplet impact test, the D.C. geared motor pushed the micrometer syringe at very slow velocity to drop an ethanol droplet. In multiple droplet impacts test, the height of the dispenser was fixed above 250 mm from the hot surface. The compressed air was supplied at 4 kPa from the pressure regulator to the liquid tank and the injection velocity u_j of 2.78 m/s was obtained. During vibrating the nozzle pipe with the moving coil, the solenoid valve was opened to start cooling of the hot surface with multiple droplet impacts. As explained before, the data sampling

system and the observation system were simultaneously started with the photo interrupter detecting a falling droplet just before impact.

Experiment repeated at the interval of over 5 minute to decay effect of previous experiment on the temperature distribution of the disk. The experimental ranges of the single and multiple impacts tests were tabulated in Tables 2(a) and (b), respectively.

Table 2 Range of experimental conditions. (a) Single droplet impact test; (b) Multiple droplet impacts test

a

Test liquid	Ethanol T_{sat} = 78 °C
Liquid subcooling ΔT_{sub} (K)	33 , 53
Nozzle inner diameter d_j (mm)	ϕ1.5
Impact velocity, u (m/s)	1.69
Diameter of droplet, d (mm)	3.7 ± 0.2
Weber number (-)	200, 370, 540
Initial surface temperature T_{so} (°C)	100 - 250
Surface inclined angle θ (deg)	0, 30, 40

b

Test fluid	Ethanol T_{sat} = 78 °C		
Liquid subcooling ΔT_{sub} (K)	53, 40, 33		
Nozzle inner diameter d_j (mm)	ϕ1.6		
Impact velocity u (m/s)	3		
Frequency of nozzle vibration f_n (Hz)	280	560	840
Diameter of droplets d (mm)	3.0	2.5	1.3
Initial surface temperature T_{s0} (°C)	160-210		
Surface inclined angle θ (deg)	30		

3. Experimental results and discussions

3.1. Response time of the thin film-wire thermocouple

To evaluate response time of the film-wire thermocouple, single droplet impact on the hot junction was first conducted under non-boiling condition. Since all the hot junctions were grounded on the disk, inductive noise from power lines was superimposed on the EMF signals from the junctions. High speed sampling of EMF signals at high gain amplification requires an appropriate signal pre/post processing such as low-pass filter (LPF). We decided appropriate cut-off frequency of the LPF based on the measured data.

Figure 4 shows effect of a cut-off frequency of LPF instrumented in the isolation amplifier on sampled temperature histories. The reference time t = 0 s was taken as the liquid-solid contact time. The line depicted as "Through" is for all-pass filter and lines denoted as 1, 10 and 100 kHz are for corresponding cut-off frequencies. It is noted that reference point of the vertical axis for each history was shifted as 3 K for convenience of comparison but the temperature scale of 2 K was fixed for each curve. Initial surface and ethanol droplet temperatures were 65 °C and 25 °C. Just after liquid-solid contact (t = 0), the sudden drop in each temperature history was recorded. The history for all-pass filter indicates that the amplitude of high frequency noise component is as large as about 1.5 K. As the cut-off frequency becomes lower, the noise component was strongly attenuated, but a response time to reach the quasi-steady temperature was getting worse from 45 μs to 480 μs.

For reference, the exact solution solid temperature distribution of 1D transient heat conduction after sudden contact of semi-infinite liquid and solid with ratio of solid and liquid thermal inertias $\beta = [(\rho_s c_s k_s) / (\rho_l c_l k_l)]^{1/2}$ =25.2 is given in Eq.(11). Thermal properties of nickel and ethanol can be referred in Table 1. In case of nickel solid

and ethanol liquid contact, the response time at $x = \delta$ (3 μm) in nickel is expected as about 50 μs. Looking at the history for 100 kHz, we can see that the response times was 75 μs and it did not deteriorated so much as compared with the results of the lower frequencies. The nose component was also appropriately eliminated. Thus the cut-off frequency of 100 kHz can was fixed for entire of the present experiments.

$$\frac{T_s(x,t)-T_l}{T_{so}-T_l}=\frac{\beta}{1+\beta}\cdot\left\{1+\frac{1}{\beta}erf\left(\frac{x}{2\sqrt{a_s t}}\right)\right\} \tag{11}$$

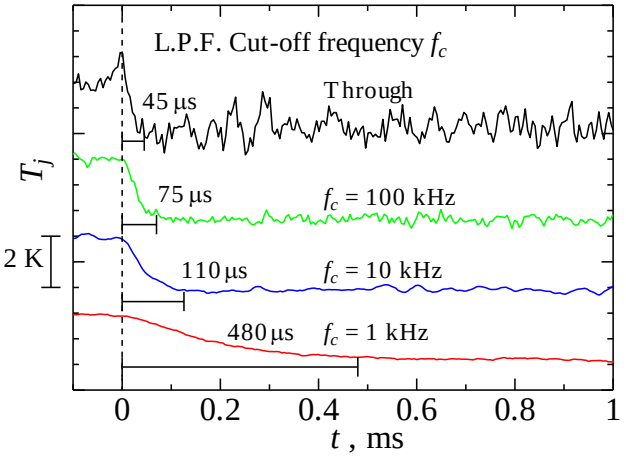

Fig.4 Effect of cut-off frequency on measured temperature response during sudden contact of a sessile ethanol droplet under non boiling situation.

3.2. Experimental results of single droplet impact tests

3.2.1. Visual observation

Figures 5, 6 and 7 show photographs of developing boiling phenomena taken for three initial surface temperatures of 140 °C, 180 °C and 230 °C. The corresponding initial wall superheats are 62 K, 102 K and 152 K, respectively. A blue dot denotes the location and real size of a hot junction. Only the initial temperature of 230 °C exceeds the spontaneous nucleation temperature of ethanol, 197 °C. A time denoted below each photo indicates the elapsed time after a droplet contacted with the reference hot junction. After droplet impact, a droplet was flattened and spread on the hot surface.

In Figs. 5(a) and (b), nucleation boiling was observed on the hot surface. Small bubbles generated and grew at active nucleation sites (Fig.5 (a)) and then coalesced to form secondary bubbles beneath the liquid film (Fig.5 (b)). Collapses of coalescence bubbles triggered generation of a small dry patch area on the surface. As indicated with the red arrows in Fig. 5 (c), the dry patches expanded to wedge away a thin bottom liquid layer and the fish net structures were formed on the surface. Finally, a liquid layer was split into spheroidal droplets as shown in Fig. 5(d). A dense mist was also generated due to intermittent contacts of droplets with the surface. As the result of the observation for the hot surface of 140 °C, nucleate boiling, namely wetted situation can be maintained until the fragmentation of the liquid film into small droplets.

Figure 6 shows development of boiling at the surface temperature of 180 °C. Active bubble nucleations on the liquid-solid interface were also observed in Fig.6 (a). However, bubble nucleation density became much larger as compared with Fig.5 and rapid coalescence of the small bubbles was observed. The partial dryout, namely the partial film boiling areas coexisted with the partial nucleate boiling areas on the surface as shown in Fig. 6(b). Then partial nucleate boiling areas shrank and disappeared, and then thin vapor blanket covered on the hot surface in Fig. 6(c). Thus Figs. 6(b) and (c) correspond to transition boiling and film boiling regions, respectively. The thin liquid film

suddenly broke from a certain point near the reference hot junction and the hot surface beneath the liquid film was exposed to atmosphere.

The vapor film generation process under a droplet dramatically changed at the surface temperature of 230 °C. Nucleation boiling was not seen except for the first contact area in Figs. 7(a) and (b). Weak nucleate boiling took place on the first contact area in Fig. 7(b). The vapor film under the droplet was quickly generated as compared with lower initial surface temperature in Fig.6. We could not observe the bubble nucleation process on the other area such as Fig.6 from pictures taken at 45 μs interval. The fact of the measured vapor film generation delay time within 45 μs implies the spontaneous nucleation process as reported by Okuyama, et al.[18] and Hassan, et al.[19]. The nucleation area was gradually weakening due to evaporation of the residual liquid layer and finally disappeared. Then fully developed film boiling was observed in Fig.7(c). The liquid film was finally broken at 8.68 ms as shown in Fig. 7(d).

From the comparison of Figs.5, 6 and 7, the surface dryout process, namely transition to film boiling situation c a n

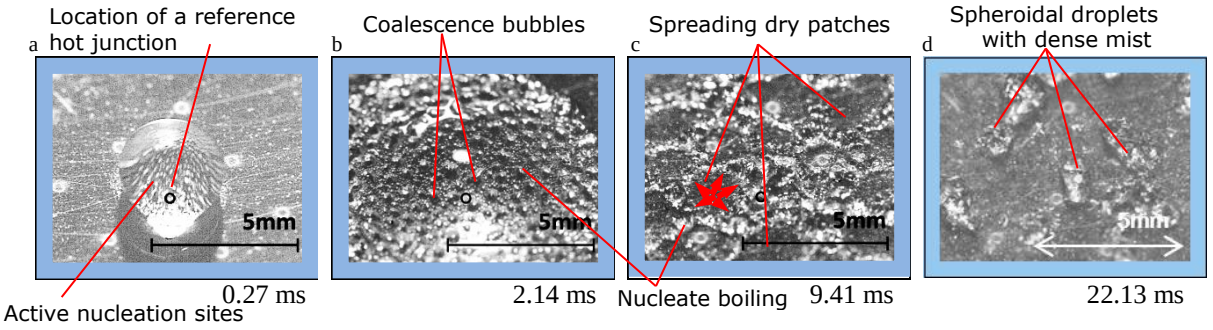

Fig. 5 Development of boiling situation at the condition of u = 1.69 m/s, ΔT_{sub} = 53 K, T_{s0} = 140 °C. (a) Nucleation of bubbles; (b)Developed nucleate boiling; (c) Breaking liquid film into fish net; (d) Spheroidal situation.

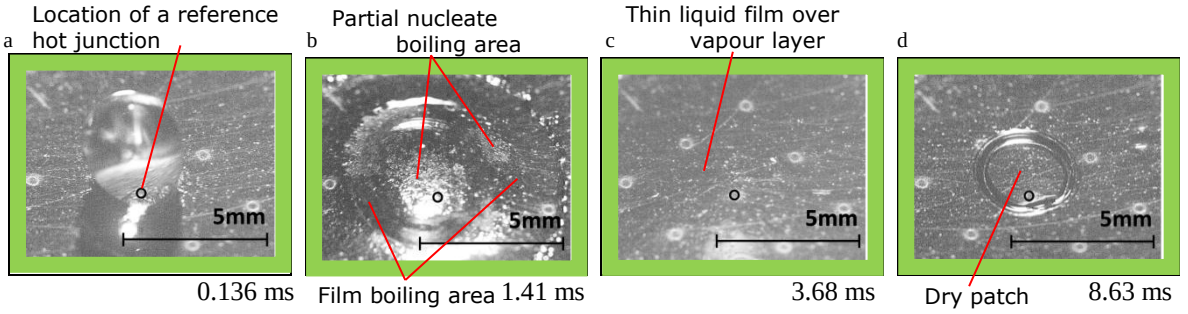

Fig. 6 Development of boiling situation at the condition of u = 1.69 m/s, ΔT_{sub} = 40 K, T_{s0} = 180 °C. (a) Nucleation of bubbles; (b)Transition boiling; (c) Developed film boiling; (d) Breaking liquid film

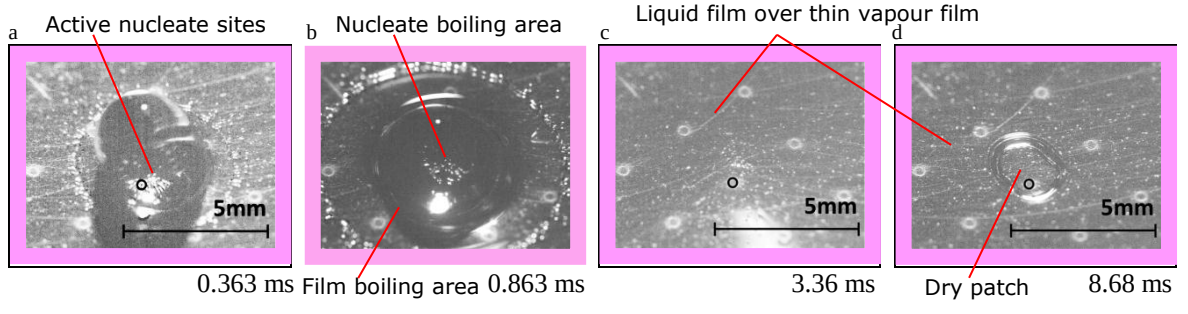

Fig. 7 Development of boiling situation at the condition of u = 1.69 m/s, ΔT_{sub} = 40 K, T_{s0} = 230 °C. (a) Nucleation of bubbles; (b)Transition boiling; (c) Developed film boiling; (d) Breaking liquid film

be categorized into three mechanisms: Type-A) breaking liquid film (fragmentation of a droplet into small spheroidal droplets), Type-B) vapor film generation with coalescence of nucleation bubbles from active nucleation sites, Type-C) rapid vapor film generation due to spontaneous nucleation such as vapor explosion. After sudden contact of liquid and solid, the hot surface can maintain wetting situation before liquid film breaking or vapor film generation. In case of the Type-A, vapor film generation was never observed. However, dryout was completed before the liquid film breaking in case of the Type-B and C. Conversely, the hot surface at high intimal temperature from 100 °C to 250 °C (corresponding wall superheat from 22 K to 172 K) can keep wetting situation for a short time after sudden liquid-solid contact. Thus we regarded the liquid film breaking time and the film generation delay time as the characteristic times of the transient dryout phenomena.

3.2.2. Characteristics of liquid film breaking time and vapor film generation delay time

Figure 8 correlates the liquid film time t_{break} and the vapor film generation delay time t_{film} with the initial surface temperature T_{so} with the droplet impact velocity u of 1.69 m/s and subcooling ΔT_{sub} of 33, 40 and 53 K. In the graph t_{break} and t_{film} are denoted as the semi-solid symbols and the open symbols with range of uncertainties, respectively. For reference, the liquid superheat limit temperature [17] T_{SHL} of ethanol at 0.1 MPa is also denoted with the red dashed line.

As shown in Fig.8, t_{break} indicated minimal value of about 5 ms at T_{so} = 140 °C and approached to about 8 ms as T_{s0} increased beyond 140°C. t_{break} monotonically increased as T_{so} decreased below 140°C. As shown in Fig.5, violent nucleate boiling was observed around 140 °C and injection of bubbles from the solid surface disturbed the liquid film and enhanced the film breaking. The liquid film breaking was observed over the whole experimental range; however the vapor film generations beneath a liquid droplet took place above the lower limit surface temperatures of vapor film generation $T_{s,LF}$ denoted as the arrows in Fig.8. When T_{so} increased beyond T_{SHL} of 197 °C, t_{film} approached to a certain value below 1 ms except for ΔT_{sub} = 53 K. The liquid subcoolings ΔT_{sub} seems not to have a major effect on t_{break} and t_{film}. The $T_{s,LF}$ for ΔT_{sub} = 33, 40, 53 K were 168 °C, 173 °C and 180 °C, respectively.

In Fig.8, we can conclude that the dryout delay time below the vapor film generation limit surface temperature $T_{s,LF}$ was determined with t_{break} and it was governed with the mechanism of Type-A. The liquid film fragmentation and spheroid droplets formation were observed on the hot surface above at least 100 °C corresponding wall superheat 22 K. For the initial temperature above $T_{s,LF}$, the dryout delay time was determined with t_{film} and dryout mechanism was categorized as Type-B or C. Distinction of Type-B and Type-C was not clear on Fig.8. However, Type-C was significant at higher than T_{SHL} for the lower ΔT_{sub} of 33 K and 40 K. On the hot surface being higher than T_{SHL}, wetting situation is able to keep for a very short time of t_{film} below 1 ms. In case of the hot surface below T_{SHL}, transition to the film boiling due to coalescence of bubbles can be possible above $T_{s,LF}$ which affected with the liquid subcooling and impact velocity.

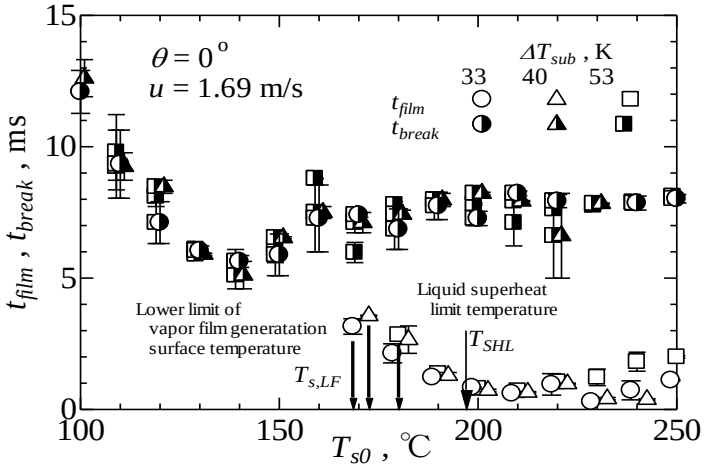

Fig.8 Effects of initial surface temperature and liquid subcooling on the film generation delay and film breaking times at the droplet impact velocity u = 1.69 m/s.

3.2.3. Histories measured temperature and inverse solutions of surface temperature and surface heat flux.

Typical measured temperature T_j, estimated surface temperature T_w and estimated surface heat flux q_w are given in Figs.9, 10 and 11. Figures 9 and 10 are given for the experimental conditions: the same initial surface temperature T_{so} of about 180 ^{o}C, the same impact velocity u of 1.69 m/s, and the different liquid subcooling ΔT_{sub} of 53 K and 40 K. Figure 11 shows the history at T_{s0} =224 ^{o}C, u = 2.0 m/s and ΔT_{sub} = 40 K. These figures correspond to the dryout mechanisms categorized into Type-A (film breaking), Type-B (vapor film blanket formed by coalescence of bubbles) and Type-C(vapor film blanket formed by spontaneous nucleation), respectively. The liquid film breaking time t_{break} and the vapor film generation delay time t_{film} are given by the arrows. Time periods denoted as "Wet" and "Dry" show the local wetting and dryout situations at the reference hot junction indicated with the red circle. The time periods denoted as "NB", "TB" and "FB" are categorized transient boiling heat transfer mode beneath the liquid droplet into nucleate boiling, Transition boiling and film boiling, respectively. The arrows denoted with (a)-(d) on the surface temperature change indicate the times when the corresponding photos shown under each graph were taken. Liquid and solid interface area beneath a droplet was color-coded to distinguish the wetted surface (blue), the dry area (yellow) and outside of liquid film (black). In the NB region the entire of the hot surface beneath the spreading liquid droplet was covered with the blue-colored wetted area. On the contrary, the hot surface in the FB region was fully covered with the yellow colored dryout area. The dryout area beneath the droplet was recognized with reduce in local heat flux and very smooth liquid film without irregular reflection of light from the liquid and vapor interface due to disturbance of bubble nucleation on the hot surface. In the TB region, partial NB and FB areas coexisted beneath the droplet and irregular and unsteady distribution of them was observed.

Liquid-solid interface temperature T_i during 1D transient heat conduction after sudden contact of the semi-infinite nickel and ethanol was denoted as the dot-dash-line in each graph. T_i is independent of time and given by Eq. (12) which is obtained by substituting x = 0 into Eq.(11). The exact solution of the surface heat flux q_i is also given as Eq.(13). It is notated that Eqs.(12) and (13) give good estimations for early stage of heat transfer just after the droplet impact with a negligible effect of phase change.

$$T_i = T_l + \frac{\beta}{1+\beta}\cdot(T_{s0} - T_l) \tag{12}$$

$$q_i(t) = -k_s \left.\frac{\partial T}{\partial x}\right|_{x=0} = -k_s \frac{T_{s0} - T_l}{(1+\beta)\sqrt{\pi a_s t}} \tag{13}$$

In Fig.9 which was categorized as the Type-A, the vicinity of the reference junction was wetted and kept nucleate boiling heat transfer until the liquid film fragmented into small droplets at 8 ms. The local temperature T_j indicated sudden drop at very high cooling rate reaching at -3x10^4 K/s just after the droplet impact and then the cooling rate after 1 ms decreased. After the local dryout due to the fragmentation of the liquid film, the T_j started to recover and approach to the initial temperature. It is noted that the periodic temperature fluctuations in T_j of about 3 K was caused by induced nose from the surroundings. Since the hot junction was so closely located to the surface, the estimated T_w was almost identical to the measured temperature T_j. The low order approximate function of T_j given as Eq.(6) was used in estimating T_w and q_w, thus the fluctuation in T_w due to the noise was considerably attenuated. T_w decreased below the liquid-solid interface temperature T_i given by Eq.(12). The surface heat flux q_w monotonically decreased with time from high heat flux beyond 10 MW/m^2 with time after and indicated almost constant value of 2-3 MW/m^2 until the local junction point kept wetting situation. Then q_w decreased to zero after the fragmentation.

In Fig.10 which was categorized as the Type-B, the hot surface beneath the droplet was completely dryout after the film generation time t_{film} of 2.5 ms and the liquid film fragmentation took place after the dryout. The major fluctuation of T_w and the sudden increase in q_w were caused by the temporary local dryout at 1.1 ms. After 2.5 ms T_w started to recover and q_w became zero, but spikes of q_w were caused by the noise included in the measured temperature. Local wetting time reduced from Liquid-solid contact time reduced from 8 ms to 2.5 ms when the liquid subcooling ΔT_{sub} reduced from 53 K to 40 K. Thus maximum drop in T_w reduced as compared with Fig.9. It

was found that the film boiling situation could maintain on the hot surface whose temperature Even though T_w was about 25 K below the liquid super heat temperature T_{SHL} of 197 °C.

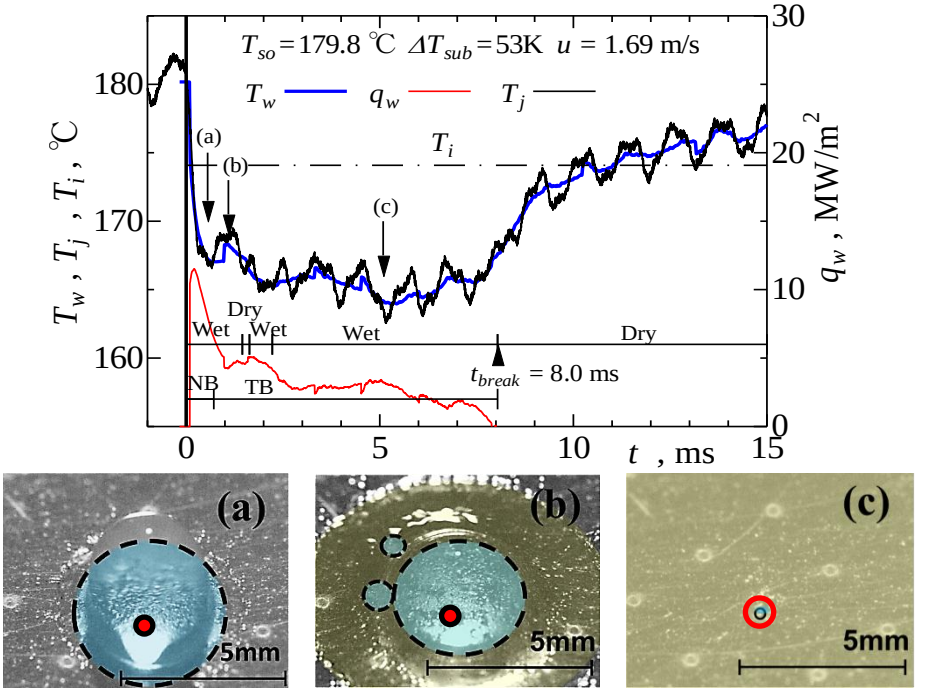

Fig.9 Typical changes of measured temperature T_j, estimated surface temperature T_w and surface heat flux q_w, with time. (Type-A, u = 1.69 m/s, ΔT_{sub} = 53 K, T_{s0} = 179.8℃)

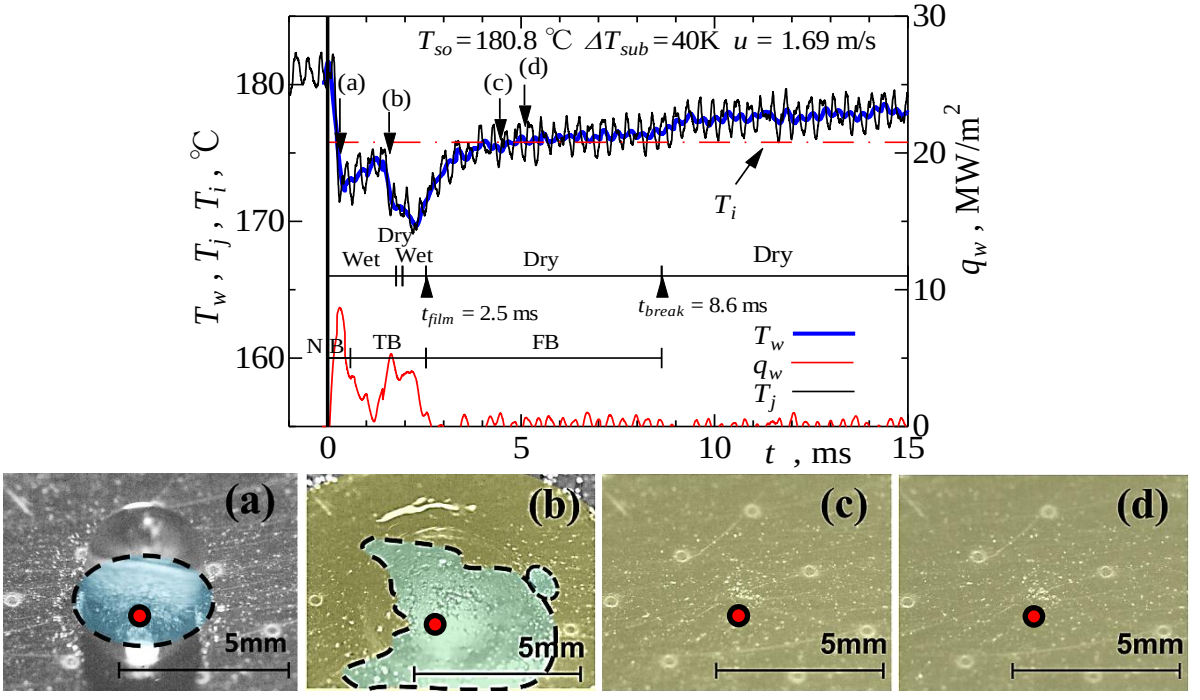

Fig.10 Typical changes of measured temperature T_j, estimated surface temperature T_w and surface heat flux q_w, with time. (Type-B, u = 1.69 m/s , ΔT_{sub} = 40 K, T_{s0} = 180.0℃)

In Fig.11 which was categorized as the Type-C, the local wetting situation kept for only 38 μs. Thus the major drop in T_w stopped at 7 K and never dropped below the T_{SHL} (197 °C) and the recovery surface temperature almost reached at the initial temperature after 15 ms. In this condition nucleate boiling on the entire surface beneath the droplet never observed within the frame interval of 44.4 μs. The minimal temperature of T_w at t_{film} was comparable with T_i. After t_{film} the heat was transmitted from the hot surface to the liquid via the thin vapor film, T_w indicated about 5 K higher than T_i. After transition to the film boiling, q_w recorded about 1 MW/m^2 until the liquid film was broken on the reference point at 8.7 ms.

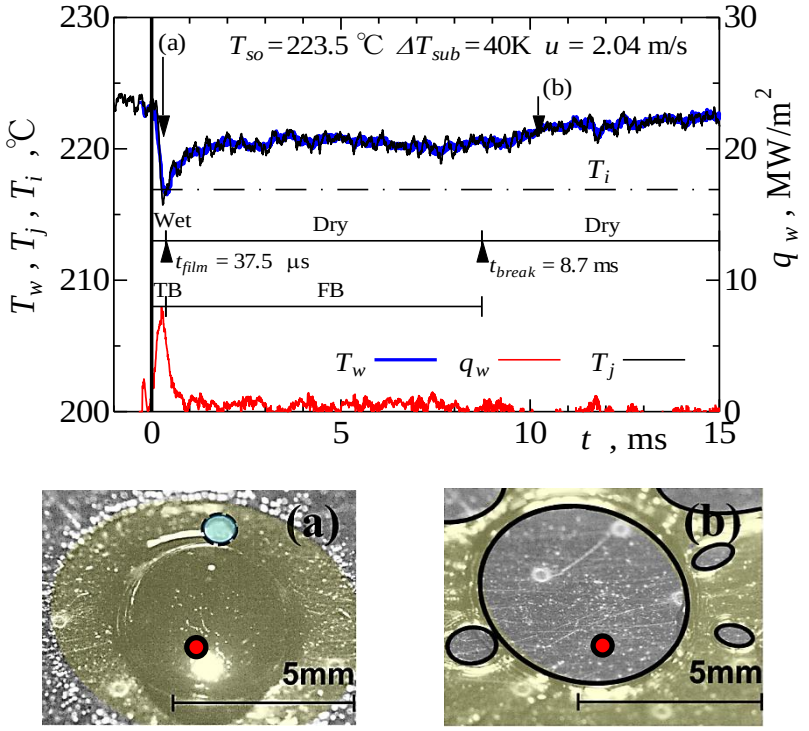

Fig.11 Typical changes of measured temperature T_j, estimated surface temperature T_w and surface heat flux q_w, with time. (Type-C, u = 2.0 m/s, ΔT_{sub} = 40 K, T_{s0} = 223.5℃)

3.3. Experimental results of multiple droplet impacts tests

3.3.1. Histories measured temperature and change in boiling situation

In Fig. 12 typical measured temperature changes during the multiple droplet impacts tests are given for three different initial temperatures; T_{s0} = 170, 180 and 190 °C. The fixed experimental conditions are the liquid subcooling ΔT_{sub} of 53 and the nozzle vibration frequency f_n of 560 Hz. The time periods denoted as “NB”, “TB”, “FB” indicate time durations of nucleate boiling, transition boiling and film boiling, respectively. The three photos taken at 34 ms, 90 ms and 799 ms were shown for T_{s0} = 180 °C. Each photo denotes the boiling situation just before impact of the next droplet and the droplet to impact next can be seen above the hot surface.

As shown in Fig.12, Similar fluctuation of the measured temperature with the single droplet impact tests was repeated in accordance with droplet impact. The film boiling was observed only at T_{s0} = 190 °C among the three initial temperatures. In case of T_{s0} = 170 and 180 °C, the transient cooling was initiated from the transition boiling. In the film boiling, the temperature fluctuation of an impact period was characterized by a flash drop in the temperature and following temperature recovery due to the formation of the vapor film. When the heat transfer

shifted to the transition boiling, duration of temperature drop gradually increased with increase in the droplet impact time and decrease in the temperature. Consequently amplitude of the temperature fluctuations increased at the transition boiling region. On the contrary, the temperature recovery disappeared on the nucleate boiling region at which the surface was wetted continuously and then temperature fluctuations in accord with the droplet impact became invisible in the temperature histories.

In the photo (a) corresponding to the end of TB region, we can see the entire of the hot surface was covered with the vapor film beneath the liquid layer film before impact of the next droplet. In the photos (b) and (c) corresponding to NB region, the nucleate boiling area was continually observed until the next droplet impacted on the surface. The photo (b) taken at the earlier NB region shows that the nucleate boiling took place on only central area around the first contact point, but the photo (c) at the fully developed NB region denoted that the entire of the liquid-solid interface was covered with NB region until the next impact.

From the experimental results of the multiple droplet impacts, we can see that the vapor film generation time gradually increases with time and finally the NB heat transfer over the entire of the droplet impact interval can be achieved. To keep the FB situation on the hot surface, microsecond order of very short t_{film} is required. Thus we considered t_{film} as a key parameter governing the rewetting phenomena under the periodical liquid-solid contacts, and tracked t_{film} at every droplet impacts until the hot surface became continuously wetted situation.

Figure 13 shows that the t_{film} during the multiple droplet impacts are correlated with initial surface temperature T_{w0} for the initial solid temperatures of T_{s0} = 170, 180 and 190 °C. The initial surface temperature T_{w0} was taken as the surface temperature at the time when droplet impacted on the reference hot junction. The relationship between t_{film} and T_{s0} at θ = 30 deg. For reference, the superheat limit temperature of ethanol T_{SHL} and the lower limit temperature of vapor film generation $T_{s,LF}$ for the single droplet test were denoted with the arrows. The dot-dash line indicated nominal period of the multiple droplet impacts $1/f_n$ = 1.8 ms. It is noted that the impact periods were sometimes fluctuated due to the coalescence or fragmentation of droplets before impact on the surface. Thus some solid symbols of t_{film} were beyond the dot-dash line.

It was also found that the t_{film} for the multiple impacts were still recorded below the lower limit temperature of the vapor film generation $T_{s,LF}$ for the single droplet impact. In a similar way as the single impact tests, the t_{film} increased with decrease of T_{w0}. In case of $T_{w0} > T_{s,LF}$, the t_{film} for the multiple impacts seem to approach to that of the single

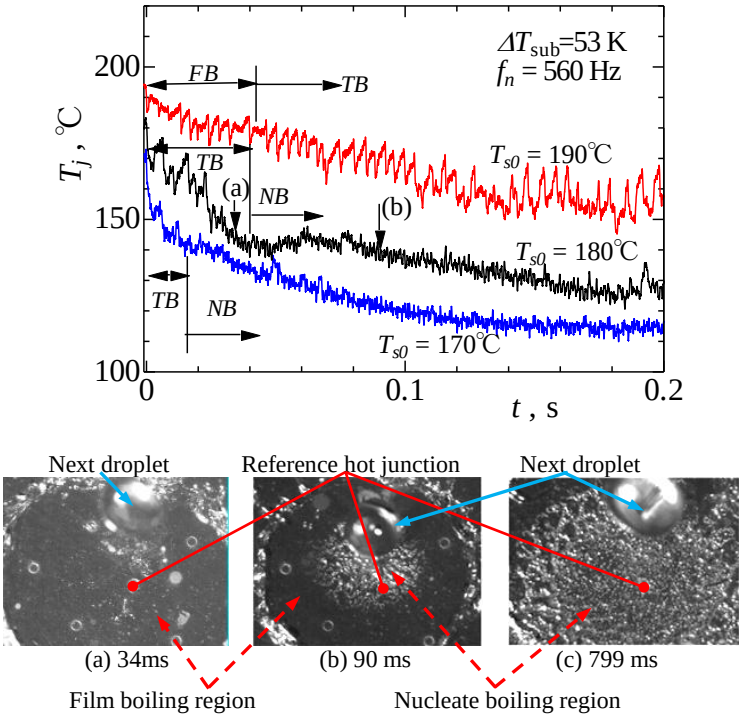

Fig.12 Cooling curve and boiling situations for T_{so} = 180 °C, f_n = 560 Hz, ΔT_{sub} = 53 K

droplet impacts denoted with the solid blue line. These facts imply that the vapor film generation delay time is not governed with only initial surface temperature in the multiple impact conditions and the transition boiling can be maintained at lower initial surface temperature T_{w0} than $T_{s,LF}$ obtained for the single droplet tests. Comparing t_{film} of the multiple impacts with the dot-dashed red line (the droplet impact period), we can see the ratio of the wet and dry duration times decreased as T_{w0} decreased. When T_{w0} of the initial solid temperature T_{s0} = 170, 180 and 190 °C decreased below 142, 145 and 170 °C, the wetting ratio reached at unity and the continuous wetting situation was achieved on the hot surface. Therefore, when the impact period reduces, the ratio of wetting duration time to the period may increase. It is expected that wetting situation is possible at higher surface temperature when the droplet impact frequency is increased.

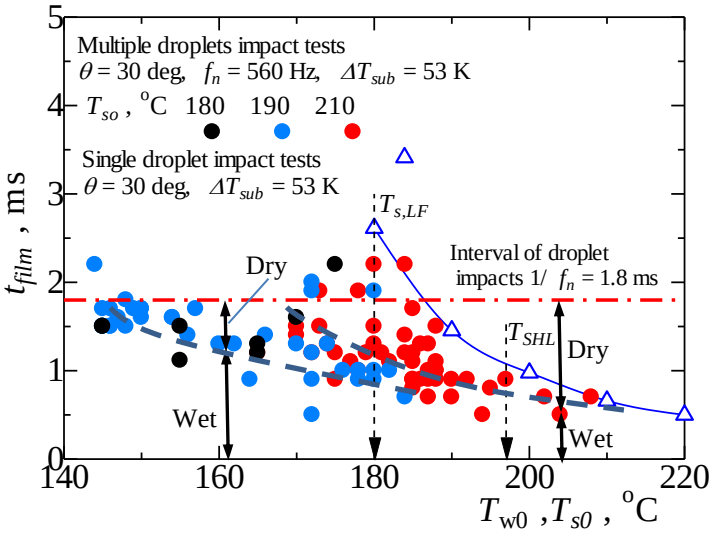

Fig.13 Relationship between the film generation time t_{film} and the initial surface temperature T_{w0} for different initial solid temperature T_{s0} during the multiple droplet impacts. (Comparison of the multiple results with the single impact)

4. Conclusions

In this study the experimental methodology to elucidate transient transition boiling on a hot surface has been developed. The combination of the developed fast response surface temperature technique, the inverse heat conduction analysis and the high speed imaging technology promises to bring us better understanding characteristics of very complicated transient boiling process as well as wetting phenomenon during quenching of hot surface.

As the first step of the research project, transient boiling processes beneath a sessile ethanol droplet produced by single droplet impact on the hot surface were carefully observed. It was found that the dryout mechanism on initially wetted surface was categorized into the three types which correspond to liquid film breaking and fragmentation of the liquid film into spheroid state droplets (Type-A), vapor film generation by coalescence of nucleation bubbles (Type-B), and very fast vapor film generation by the spontaneous nucleation (Type-C). Each dryout process was required a certain film generation delay time from a couple ten millisecond to microsecond. In case of type-B and C which were observed around / above the liquid superheat limit temperature, the hot surface could keep the wetting state for the vapor film generation time. The relationships of the film generation time and the initial surface temperature for the multiple droplet impacts indicated a similar trend but the film generation time for the multiple impacts was recorded below the lower limit initial solid temperature of the single impact test. This fact may give one of the interpretations about the wetting temperature shift to higher wall superheat region commonly known in laminar and spray quenching.

Acknowledgements

This work was supported by JSPS Grant Numbers 20253586 and 22560204. Mr. Yuhei Kojima and Ms. Narumi Koto also helped to build the experimental apparatus and perform the experiments. The authors gratefully acknowledged their supports.

References

[1] Nukiyama, S., The maximum and minimum values of the heat Q transmitted from metal to boiling water under atmospheric pressure, Int. J. Heat and Mass Transfer, 9 (1966) 1419-1433.
[2] Groendes, V. and Mesler, R., Measurement of Transient Surface Temperatures beneath Leidenfrost Water Drops, Heat Transfer, 4 (1982) 131-136.
[3] Lee, L.Y.W., Chen, J.C. and Nelson R.A., Liquid-Solid Contact Measurements Using a Surface Thermocouple Temperature Probe in Atmospheric Pool Boiling Water, Int. J. Heat Mass Transfer, 28 (1985) 1415-1425.
[4] Dennis N. Assanis, Francis A. Friedmann, A thin-film thermocouple for transient heat transfer measurements in ceramic-coated combustion chambers, Int. J. Heat Mass Transfer, 20 (1993) 459-468
[5] Nakabeppu, O., Wakasugi, H., Approach to Heat Transfer Mechanism beneath Single Boiling Bubble with MEMS Sensor, Proc. of 13th International Heat Transfer Conference, BOI-43 (2006). (in CD-ROM).
[6] Moore, F. D. and Mesler, R. B, The measurement of rapid surface temperature fluctuations during nucleate boiling of water, AIChE Journal, 7 (1961) 620-624.
[7] Yu, C.L and Mesler, R.B., A Study of Nucleate Boiling near the Peak Heat Flux Through Measurement of Transient Surface Temperature, Int. J. Heat Mass Transfer, 20 (1977) 827-840.
[8] Buchholz, M., Lüttich, T., Auracher, H. and Marquardt, W., Experimental investigation of local processes in pool boiling along the entire boiling curve, Int. J. Heat and Fluid flow, 25 (2004) 243-261.
[9] Heichal, Y., Chandra, S and Bordatchev, E., A first-response Thin Film Thermocouple to Measure Rapid Surface Temperature Changes, Experimental Thermal and Fluid Sc., 30 (2005) 153-159.
[10] Mohammed, H., Salleh, H. and Yusoff, M.Z., Design and Fabrication of Coaxial Surface Junction Thermocouples for Transient Heat Transfer Measurements, Int. Comm. in Heat Mass Transfer, 35 (2008) 853-859.
[11] Marr, M.A, Wallace, J.S, Chandra, S., Pershin, L. and Mostaghimi, J., A Fast Response Thermocouple for Internal Combustion Engine Surface Temperature Measurements, Experimental Thermal and Fluid Sc., 34 (2010) 183-189.
[12] Liu, W. and Takase, K, Development of measurement technology for surface heat fluxes and temperatures, Nuclear Eng. and Design, 249 (2012) 166-171.
[13] Monde, M., Analytical Method in Inverse Heat Transfer Problem Using Laplace Transform Technique, Int. J. Heat Mass Transfer, 43 (2002) 3965-3975.
[14] Woodfield, P., Monde, M. and Mitsutake, Y., Improved analytical solution for inverse heat conduction problems on thermally thick and semi-infinite solids, Int. J. Heat Mass Transfer, 49 (2006) 2864-2876.
[15] Carslaw, H.S., Jaeger, J.C., Conduction of Heat in Solids, 2nd Ed., Oxford University Press, Oxford, 1952.
[16] Japan Society of Thermophysical Properties, Japan Thermophysical properties handbook, Yokendo co. ltd., Tokyo, 2007.
[17] Lienhard J,H. , Correlation for the limiting liquid superheat, Chemical Engineering Science, 31 (1976) 847-849.
[18] K. Okuyama, S. Mori, K. Sawa, Y. lida., Dynamics of boiling succeeding spontaneous nucleation on a rapidly heated small surface, Int. J. Heat Mass Transfer, 49 (2006) 2771-2780.
[19] M.N. Hasan, M. Monde, Y. Mitsutake, Homogeneous nucleation boiling during jet impingement quench of hot surfaces above thermodynamic limiting temperature", Int. J. Heat Mass Transfer, 54 (2011) 2837-2843.

The Advanced Technology and Future Prospect of OTEC in Japan and the World

- for Stable Energy &Sustainable Water Resource-

Yasuyuki Ikegami, Saga University, Japan

Europe and America and Korea have been promoted the practical use of the marine renewable energy forward on a large scale project by the strong leadership of these governments while an energy problem and an environmental problem of the 21st century on a global scale have been increasing in the acuteness and emergency degrees. The renewable ocean energy (ROE) is strongly expected worldwide at practical use to be next to photovoltaic power generation, wind power generation as enormous energy resources and a point of the job creation.. The activity of Japan on ROE has been evaluated as world top-level at the laboratory level, by the way, Japan is delayed in the actual large proof R&D in the sea area in the other countries more than ten years. Recently, Japan with a few resources has begun to be aimed at the innovation of the ROE development full-scale as the sixth useful area in world, so-called exclusive economic zone (EEZ). This year, the NEDO announced the technical road map toward 2030 of ROE including ocean thermal energy conversion(OTEC) and the wave power generation.

Saga University has investigated on REO as only COE on REO in the whole country. Especially, OTEC has been researched as aim at the practical use for about 40 years. OTEC is a system generating electricity with temperature difference between warm sea water of the ocean surface and the cold sea water from depths 600m to 1,000m. The 30kW OTEC device which Saga University has is evaluated on as the device that performance is the highest now in the world. The characteristic of OTEC is stable and multi-purpose, not only the electricity but also seawater water conversion, hydrogen production, lithium collection, the fishing ground reproduction is possible. Saga university has contributed to the development of sustainable energy and water resources that these Japanese technology is asset to the project in U.S.A., France, India, Taiwan now In this session, the current status and future prospect are presented on ROE, mainly on OTEC.

Desalination using Ocean Thermal Energy in India(100t/day)

NEDO(New Energy and Industrial Technology Development Organization)

NEDO

7. OTEC ～Technology Roadmap～

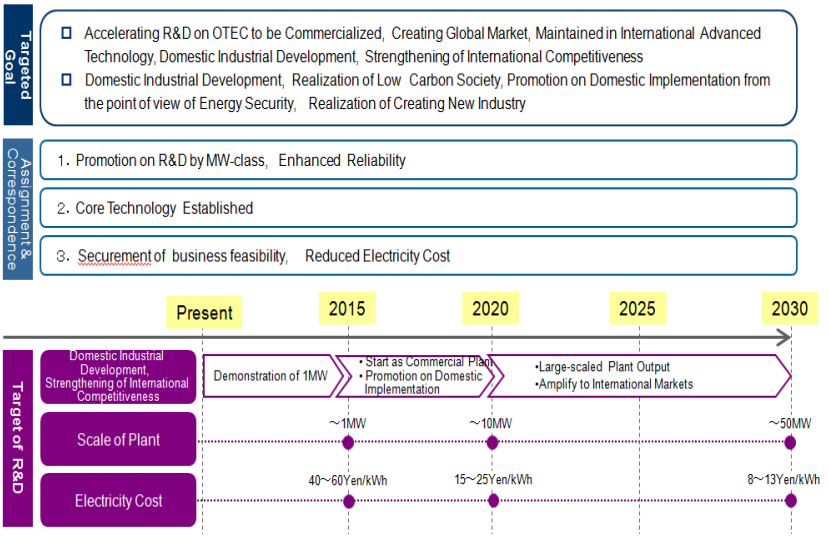

9

CFD, In vivo and In vitro Studies for Biofluid Circulations

Dr. Ing. Suh, Sang-Ho

Dept. of Mechanical Engineering, Soongsil University, Seoul, Korea

Abstract

Arterial diseases are being increased and the pathogenesis of hemodynamic mechanism of the development and progression of vascular disorders such as atherosclerosis and aneurysm are being investigated. Development of clinical diagnostic techniques has been so limited to define the pathobiological role of atherosclerosis. FSI (Fluid Structure Interaction) and flow visualization is a good tool to analyze the vascular flow patterns. CFD, FSI and In vitro experiment can helps to predict pathogenesis of the biofluid circulation problems and also applied to development of clinical diagnostics technique. Atherosclerosis is a progressive disease characterized by inflammation and lipid accumulation in the vascular wall, Obstructive sleep apnea (OSA) is a syndrome characterized by repetitive episodic collapse of the upper airway, and ureter obstruction occurs when urine flows in parallel in the bore and in the surrounding annulus of a stent. The purpose of this study is to analyze flow patterns in the left coronary artery, upper airway, and ureter using numerical and experimental techniques. Here we analyzed flow patterns and hemodynamic factors using numerical techniques. We analyzed FSI (Fluid Structure Interaction) simulations in the left coronary artery, upper airway, and ureter double J-stent 3D models which were carried out from CT scanned images and meshing done by CFD. The inflow and outflow boundary conditions were applied from CT data for flow analysis. A Navier-Stokes governing equations were discretized by finite volume method for numerical simulations. FSI analysis were performed of left coronary artery to get the hemodynamic factors and flow visualization done by rapid prototype model, obstructive sleep apnea performed flow characteristics in the upper airway to emerging concepts of ventilator control mechanisms in the normal sleep apnea versus sleep disordered breathing, and ureter obstruction flow analysis of the effects of the ureteral wall compliance, the pressure difference between the ureteral inlet and outlet. In the coronary RP model, Young's modulus and movement of coronary artery which affect hemodynamic and accordingly has an effect on atherosclerosis, and The magnitude of the pressure gradient is regarded as the pressure effort required for breathing and extent the reduction of pressure effort in the upper airway. These all results can be used to develop of clinical diagnostics techniques.

A new approach to anisotropy in wall-turbulent shear flow, and with application to organised disturbances, when these are present

P. K. Sen, Srinivas V. Veeravalli, S. Hegde and Ganapati Joshi
Department of Applied Mechanics, Indian Institute of Technology
Delhi, New Delhi 110-016, India.

Abstract

This paper takes a re-look at anisotropy in wall-turbulent shear flow, from the viewpoint of the primitive equations for turbulence, i.e. without considering averages. The paper attempts to develop some simple rules for the anisotropic part, and arrives at a logical definition of eddy viscosity and the turbulent shear stress tensor. The results are extended to the constitutive equation for organised disturbances in turbulent shear flows, when such disturbances are present. The model of Sen and Veeravalli (Sadhana 1998, 2000, 2007), for organised disturbances, seems to be vindicated.

Available online at www.sciencedirect.com

ScienceDirect

Procedia Engineering 00 (2015) 000–000

Procedia Engineering

www.elsevier.com/locate/procedia

6th BSME International Conference on Thermal Engineering (ICTE 2014)

A Micro Industry with Closed Energy and Water Cycles for Sustainable Rural Development

Padma Vasudevan Sen*[a], P.K. Sen[a], S. Hegde[a], S.N. Singh[a], A. Mukhopadhyay[b], Prahalad Singh[c], Philip Davies[d], R. Berry[d], P. K. Dey[d] and Cyrus Engineer[e]

[a]*Department of Applied Mechanics, Indian Institute of Technology, Delhi, India*
[b]*Department of Science and Technology, Delhi, India*
[c]*School of Desert Sciences, Jodhpur, Rajasthan, India*
[d]*Aston University, Birmingham, U.K.*
[e]*IB Turbo Limited, New Delhi, India*

Abstract

Sustainable development requires combining economic viability with energy and environment conservation and ensuring social benefits. It is conceptualized that for designing a micro industry for sustainable rural industrialization, all these aspects should be integrated right up front. The concept includes; (a) utilization of local produce for value addition in a cluster of villages and enhancing income of the target population; (b) use of renewable energy and total utilization of energy generated by co and trigeneration (combining electric power production with heat utilization for heating and cooling); (c) conservation of water and complete recycling of effluents; (d) total utilization of all wastes for achieving closure towards a zero waste system. *Enhanced economic viability and sustainability is achieved by integration of appropriate technologies into the industrial complex.*

To prove the concept, a model Micro Industrial Complex (MIC) has been set up in a semi arid desert region in Rajasthan, India at village Malunga in Jodhpur district. A biomass powered boiler and steam turbine system is used to generate 100-200 KVA of electric power and high energy steam for heating and cooling processes downstream. The unique feature of the equipment is a 100-150 kW back-pressure steam turbine, utilizing 3-4 tph (tonnes per hour) steam, developed by M/s IB Turbo. The biomass boiler raises steam at about 20 barg 3 tph, which is passed through a turbine to yield about 150 kW of electrical power. The steam let out at a back pressure of 1-3 barg has high exergy and this is passed on as thermal energy (about 2 MW), for use in various applications depending on the local produce and resources. The biomass fuel requirement for the boiler is 0.5-0.75 tph depending on its calorific value. In the current model, the electricity produced is used for running an oil expeller to extract castor oil and the

* Corresponding author. Tel:+91-9810433251
Email address: padmav10@gmail.com

Peer-review under responsibility of organizing committee of the 6th BSME International Conference on Thermal Engineering (ICTE 2014).

castor cake is used as fuel in the boiler. The steam is used in a Multi Effect Distillation (MED) unit for drinking water production and in a Vapour Absorption Machine (VAM) for cooling, for banana ripening application. Additional steam is available for extraction of herbs such as mint and processing local vegetables.
In this paper, we discuss the financial and economic viability of the system and show how the energy, water and materials are completely recycled and how the benefits are directed to the weaker sections of the community.

Peer-review under responsibility of organizing committee of the 6th BSME International Conference on Thermal Engineering (ICTE 2014).

Keywords: Trigeneration; Micro-industry; Sustainable development

1. Introduction

It is now well recognized that economic growth alone does not lead to sustainable development. Besides techno-economic viability, we must simultaneously address energy, environment, water and social issues which are needed for sustainability. Conservation of human values and the ethical fabric of the society is an additional dimension. Industrialization must be planned within this framework assessing the technological system holistically.

Energy is a key input to mechanization. Ecofriendly and decentralized, renewable energy resources such as biomass and solar are most suitable for rural areas where there is good sunshine and conditions support agriculture. Generally, biomass is available and accessible in the form of residues from agriculture and various agro based industries besides dedicated energy plantations. Enterprises based on these resources may be developed at different scales from household to village clusters as shown in Figure 1.

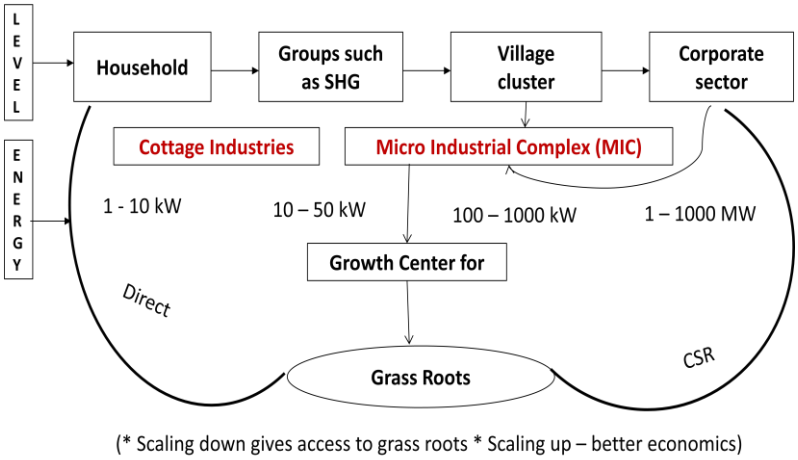

Fig. 1: Sustainable Enterprises at different scales

Both capital investment and energy requirements are scale specific. While, returns for investment would be higher at bigger scales of operation, at smaller scales there is a greater potential for local value addition and fostering employment and equity among the weaker sections. Hence, for achieving sustainability and spread effect, technologies and systems which are economically viable at small and intermediate scales have to be designed, developed and implemented at selected sites. Such scales are also suitable for designing closed energy, water and material cycles for environmental conservation.
Cogeneration and trigeneration help in the operation of closed-energy cycles. In the co and trigeneration mode, primary energy in the fuel is converted into electricity and thermal energy. The latter is used for heating and cooling in trigeneration. Thus, a broad range of energy services are made available at site. The systems can be configured and implemented in many ways, depending on the energy source, product and process requirements and the scale of

operation. Some examples have been listed in an earlier publication by the authors [1, 2].
Given the water scarcity at global levels, conservation and efficient utilization of water resources are of universal importance. Water of different quality and quantity is needed for drinking, domestic consumption, agricultural, industrial and other applications. The global demand is increasing with population and quality of life. Irrigation accounts for major water consumption in an agricultural economy. On the other hand, any industrial enterprise will necessarily consume water. The effluents from the industry have to be suitably treated for use within the premises for e.g. cleaning and for irrigation of land nearby for biomass production.
In general, to minimize footprints on the environment all efforts must be made to conserve and recycle all materials and wastes, solid, liquid and gaseous. For example, organic waste can be treated by chemical or bio chemical pathways to generate bio fuels, bio fertilizers, bio pesticides etc. or dried and pelletized for use as fuels.

2. Designing a Sustainable System

Within the above broad framework the design of the industry has to be based on site specific factors. To begin with we list out all the raw materials, energy resources and technologies available for energy conversion and utilization, processing of materials and waste management at the scales of operation desired. The technologies appropriate to the site and scale are selected and integrated to satisfy the sustainability criteria *viz* techno economic viability, energy and environment conservation and total waste recycling.

2.1 Energy from Biomass

*Biomass availability as Energy Resource: B*iomass resources may be classified under the heads agro residues, agro industrial residues and dedicated energy plantations. The quality, quantity and sustainable availability have to be considered. These vary widely with the agro climatic conditions and agro industrial base in the area.
By way of illustration, availability of biomass from selected agricultural residues and energy crops may be considered [3, 4, 5]. Agricultural crops such as rice and wheat yield about 1-3 tons per hectare of hay. Additionally when dehusked, husk and bran are available as residues. In the case of oil crops such as castor and groundnut, the seed availability under rainfed condition is around 0.5–1.5 t/ha, and the yield may be twice as much under irrigated conditions. Mostly the oil content is in the range 30-50%. Hence, while extracting oil more than 50% of the seed yield is returned in the form of oil cake. For example, it is reported that for each ton of castor oil, 1.31 ton of husk and 1.13 ton of meal are produced [6]. Further, in oil crops cultivation, stalks and other residues are also available. It has been reported that castor stalk, a by-product of castor plant cultivated for its seeds, has an average yield of 10 dry t/h, which is higher than average yield of forest in temperate zone [7].
Among energy plantations, high biomass yields of a variety of grasses have been noted. For example, switch grass (*Panicum virgatum*) and miscanthus spp. are reported to yield 5-23 tons and 5-44 per hectare of biomass respectively in a year [5]. Dedicated energy plantations of trees like Salix and Eucalyptus yield approximately 10-20 tons of wood per hectare post maturity. The yield increases considerably on irrigation especially with domestic wastewater containing nutrients [8].

2.1.1 Harnessing energy from biomass: There are a number of technologies for harnessing the chemical energy stored in biomass into other forms of energy. The pathways for energy harnessing may be classified as thermo chemical and bio chemical routes. *These include direct combustion and utilizing the heat, bio oil generation, pyrolysis, gasification and biomethanation among others.* The choice depends on the type of application and the scale of operation. These have been discussed in detail in the context of trigeneration [1]. It may be noted that among these, direct combustion of biomass in boilers for steam generation is most useful in an industry where steam is needed for processing and power is generated by a steam turbine (cogeneration).

2.2. Effluent Water and Solid Waste Recycling

It is useful to design for closed water and solid material cycles to ensure conservation. Any waste generated in liquid and solid forms can be treated and utilized for biomass production which in turn can be put back as fuel. This leads to no or low carbon footprint. Phytoremediation of waste water by passing through plants roots has emerged as an ecofriendly alternative for effluent water treatment. If waste water is devoid of toxicants it can be directly used for irrigation (also known as fertigation when waste water has considerable nutrients). In case, certain contaminants

need to be removed from the waste water, it can be passed through terrestrial constructed wetlands and floating wetlands [9, 10, 11]. Also, in water management it is useful to integrate rainwater harvesting in most sites.
As for organic solid wastes, these can be used for generating compost and vermi-compost which can be used to fertilize plants. Where, wet waste biomass is available, biomethanation is an alternative to generate nutrient rich compost besides biomass.

3. Setting up of Micro Industrial Complex (MIC): The Trigeneration system

Biomass which is a renewable resource is traditionally used in villages essentially for heating and lighting. This resource has to be made useful for providing "higher forms" of energy which can support micro enterprises. This way benefits would reach directly to the small farmers because they will be involved in the production of biomass and utilize the same locally. A conceptual framework has been developed for generating "sustainable livelihoods" using locally accessible biomass such as agro-residues, weeds and biomass grown specifically in the form of energy plantation. The process of "trigeneration" is at the heart of this system. Within this broad framework for interventions, technologies are selected and integrated depending on local specific conditions. For proving the concept MIC is set up at the village Malunga in Jodhpur district, Rajasthan. The design and initial work done has been described in our earlier publication [2]. As a sequel to this, the actual establishment of the industry is presented in detail herein.
Malunga was selected for setting up the MIC as a challenging task. The village is 37 km northwest of Jodhpur city in the rural hinterland. It falls in a semi arid zone with a rainfall less than 300mm per annum. The soil is sandy loam and groundwater is saline in many areas. The temperature in summer is very high (42 – 47°C) and sun shine is available for about 300 days. In winter the temperature falls to 10°C. There is water scarcity for drinking and irrigation in most places. Crops tolerating salinity and drought conditions are suitable for cultivation. Oil seeds e.g. castor and vegetables and fruits like tomato, Ber (Zizyphus spp) and amla (*Phyllanthus emblica)* are grown. Also aromatic herbs and spice crops like mint and cumin are cultivated. Cotton and chilli are cash crops. Opportunities for employment in agriculture and other sectors are limited. Hence, new avenues have to be opened up for income generation.

Given the above local conditions the following technologies are suitable for development of the area, where possible using local produce (table 1).

Table 1: Technology Selection for Malunga

Local Need	Technology Interventions Needed
Rainwater Harvesting	Check Dams and Rainwater Recharge, Roof top harvesting
Crushing Castor Seeds for Oil	Setting up Oil Mill
Drinking Water Production	Multi Effect Distillation (MED), Reverse osmosis (RO)
Premises Cooling	VAM Cooling, Evaporative cooling
Irrigation Conservation	Drip & Clay Pot Irrigation
Electricity and other forms of energy	Boiler and Turbine combination for co/trigeneration
Processing agricultural produce	Drying, Cooling, extraction and various food processing technologies using steam
Solar Devices for utilizing solar energy	Solar Thermal Devices for Steam Generation, Solar photovoltaic for water pumping, lighting and cooking
Income generation and value addition	Setting up an Industry for employment generation and processing local produce

The MIC was carefully designed to integrate all the above activities with synergy to create a sustainable system. School of Desert Sciences (SDS), which took the responsibility of running the MIC also helped in the design and construction. All the technologies chosen are ecofriendly and the system was designed to benefit the community in short and long terms. The schematics of the trigeneration system and product mix are shown in Fig. 2.

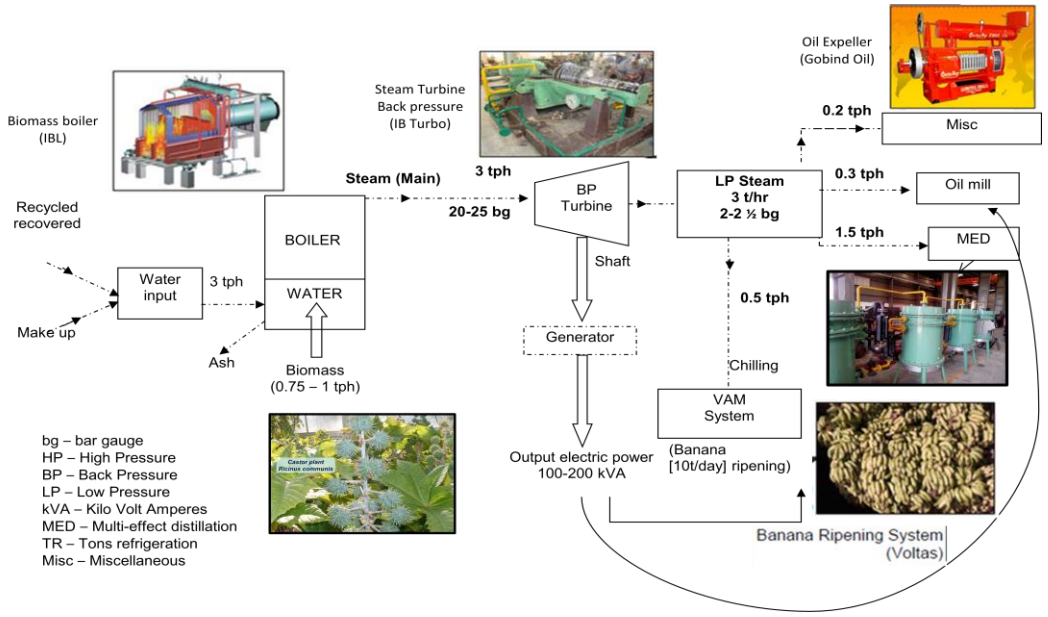

Fig. 2: MIC Model: Trigeneration System and Product mix.

3.1. Site and equipment details:

The layout and view of the site is shown in fig. 3. The workings of various individual components are discussed.

Fig. 3: Site plan and MIC View

3.2. The Boiler and Turbine:

A biomass powered boiler and steam turbine system is the main component used to generate electric power and high energy steam for heating and cooling processes downstream. The unique feature of the equipment is the 100-150 kW back-pressure steam turbines developed by M/s IB Turbo (fig. 4&5). The biomass boiler raises steam at about

20 barge 3 tph, and this steam is passed through the turbine to yield about 150 kW of electrical power. The steam is let out at a back pressure of 1-3 barg.

Fig. 4: Biomass Boiler, Turbine and VAM Set Up

The steam, which still has high exergy, passes on the latent heat as thermal energy (about 2 MW), for use in various applications, namely VAM based chilling and preparation of drinking water using Multi Effect Distillation (MED). Various other applications may be added depending on local produce and resources. In the current scenario, castor cake and castor plant residues along with locally available wood are used as fuel for the boiler. Since oil cake has a high calorific value, only 0.5- 0.7 ton of fuel may be needed to generate 3 tph of 20-25 bar gauge steam.

3.3. Castor Oil Mill:

In the current system an oil mill with a capacity to crush 30 tons of castor oil seeds per day was set up (Fig.5). The oil mill requires significant amount of electric power (80-100 kWH) and some amount of steam (0.2-0.5 tph). These are drawn from the trigeneration system. Choosing castor for production of oil under MIC has multiple benefits. There are ready markets for castor oil. The oil is a chemical feedstock for a variety of products including lubricants and pharmaceuticals. The biomass residue (stalk and leaves) can also be used as fuel. Castor seed yields can be increased by using locally available wastewater for irrigation of this non-edible crop.

3.4. Banana Ripening Plant:

Under the MIC, the VAM (based on lithium bromide and water) system was selected for ripening bananas at 16°C in an ethylene based process (http://isopaninsulation.com). Each load of banana (10-16 tons per day) is ripened in a four days cycle. Banana is brought from the neighbouring states, is ripened at one load per day and is marketed locally with an added value as profit.

a b

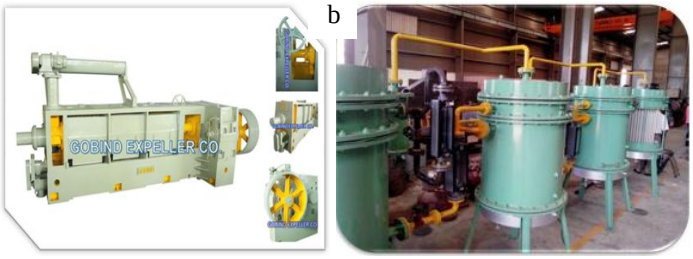

Fig. 5: (a) Oil Mill (b) MED Unit

3.5. Drinking water production by Multi Effect Distillation (MED): (Fig.5)

The other major product considered under the MIC is distilled water produced by using a small scale multi effect distillation technology [12, 13, 14 and 15]. The product water can be used for drinking water, battery water and other types of water as needed by the customer. Since ground water in the surrounding areas is saline (with TDS up to 2,000 ppm) there is a good demand for properly purified drinking water. A system for dosing, packaging and

marketing drinking water has been set up.

3.6. Other activities:

Other uses of steam envisaged are for extraction of mint for essential oils and processing of vegetables such as carrots. VAM based cooling system can provide cooling for storage of most types of the vegetables in the area.

Management of wastes such as ash from the boiler, wastewater effluents, gaseous emissions and any solid organic wastes generated are given due consideration. Ash would be used for soil amendment or cement work. Wastewater will be recycled and rejects will be concentrated in solar evaporation ponds. Saline water can be used on the pads of green house for evaporative cooling [16]. Any organic waste, such as spoilt bananas, will be composted or dried and used in boiler.

4. Ensuring Sustainability:

4.1 Financial aspects: MIC as a business solution:

The MIC was designed to be a good business solution. Revenues will be earned from services rendered for banana ripening (10 to 16tons/day) and oil expelled from castor seeds (30 tons of seed/day). In addition, the plant will have capacity to produce 50,000 one-litre bottles of packaged drinking water per day. Costs will be incurred for the bottle components (pre-forms, caps, labels) and for the fuel, and returns will be from the sale of water.

The net revenue from MIC is estimated at 1lakh Rs/day, against a total capital investment at 600 lakh rupees. Details are available in our earlier paper [2].

4.2 Energy Related Issues:

On crushing (30t/d) of castor seeds about 12t/d of oil and 18/d of caster cake are obtained. In the main boiler which can generate 3-4 tph of steam, the biomass requirement is 0.75 to 1 tph. Since oil cake has higher calorific value, the requirement of cake may be less than 0.75 tph. There is an auxiliary boiler which can generate 1tph of steam, and can be used to run VAM when the main boiler is not in operation. The oil cake requirement for this boiler is 0.2 to 0.25 tph. It is estimated that about 10-12 t/d of oil cake may be used in the boilers and surplus castor cake will be available for sale. Also castor stalks from nearby fields will be available as fuel.

Water and steam are used to carry and deliver energy for different machinery. The efficiency of the boilers in converting water to steam is about 80%. As highlighted in Fig. 2 the steam is fully utilized in the trigeneration system.

Thus above 70-75 % energy in the biomass fuel is utilised for production. Heat losses essentially occur from the chimney and the boiler, depending on the moisture content of the fuel, and from pipe work and equipment. The electricity generated by trigeneration should be sufficient for running the MIC as shown in table 2. Grid power will be used at the time when the system is switched off. Also a 125 kVA (100 kW) diesel generator is provided as back up. Research is being undertaken to run this on Biodiesel.

Table 2: Electrical Load Balance (Demand): Peak Load Profile

Unit	Installed kW	Operating kW
Oil Expeller	96	77
Bottling Plant	50	40
VAM	25	20
Boiler	30	24
Total	201	161

It may be noted further that MED saves energy. Distillation requires high initial energy inputs. It takes about 1 kWh of energy to produce 1 Kg of steam or distilled water. Recycling the latent heat of vaporisation in multi effects gives several folds of distilled water per unit steam input.

4.3 Environmental aspects:

4.3.1 *Rainwater harvesting (RWH)*: This is adopted in the MIC to replenish ground water. Rainwater is harvested from an adjacent hillside, providing about 30 hectares collection area. About 90,000m^3 per year of water could go to

the aquifer. The annual requirement of the bottling plant is 15,000m^3. Even with 20 per cent recharge efficiency, water taken from the tube well can get replenished by harvested rainwater (fig. 6).

Fig. 6: Rainwater Harvesting by SDS: Some Views of the site

4.3.2 Total water utilisation: Water is drawn by a tube well into MIC and used to raise steam in the boiler after suitable treatments. For this, water softening and RO units are integrated. Water cycle in the system is shown in Fig. 7. Water effluents are also treated and used for raising biomass.

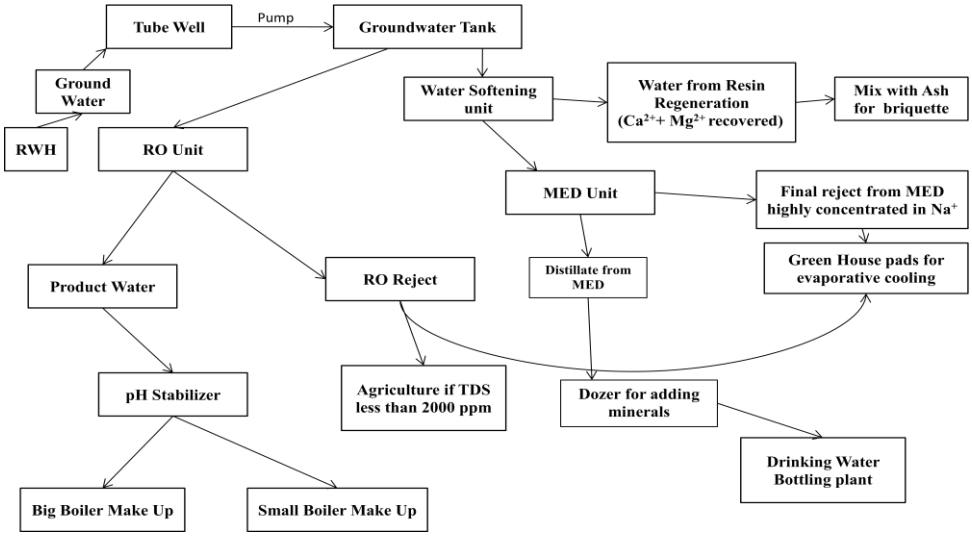

Fig. 7: The Water Cycle

Further to avoid air and land pollution, due consideration is given to chimney design for non-pollution by flue gasses and all solid and liquid wastes are recycled.

4.4 Social issues:

Use of local produce will lead to value addition and employment generation. Due to rainwater harvesting, water levels have gone up and the community is benefiting in agri- horticulture. Due to MIC set up, the village is getting better infrastructure like roads. The overall primary, secondary and tertiary impacts of MIC are shown in fig. 8.

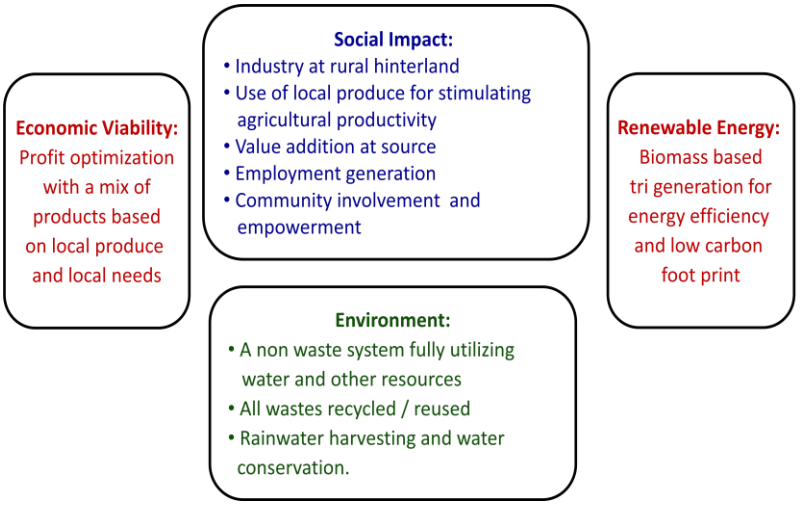

Fig. 8: Economic, Environment and Social Impacts

4.5 Future Scenario:

The unique feature of setting up of the MIC is that SDS which operates the system has pledged to deploy the profit for development of the rural areas. SDS will expand the factory production utilising steam in more activities like mint extraction and vegetable processing. Also solar energy devices will be introduced. The MIC in general can act as an anchor for development of the surrounding villages for awareness generation, training and technology transfer as shown in fig. 9.

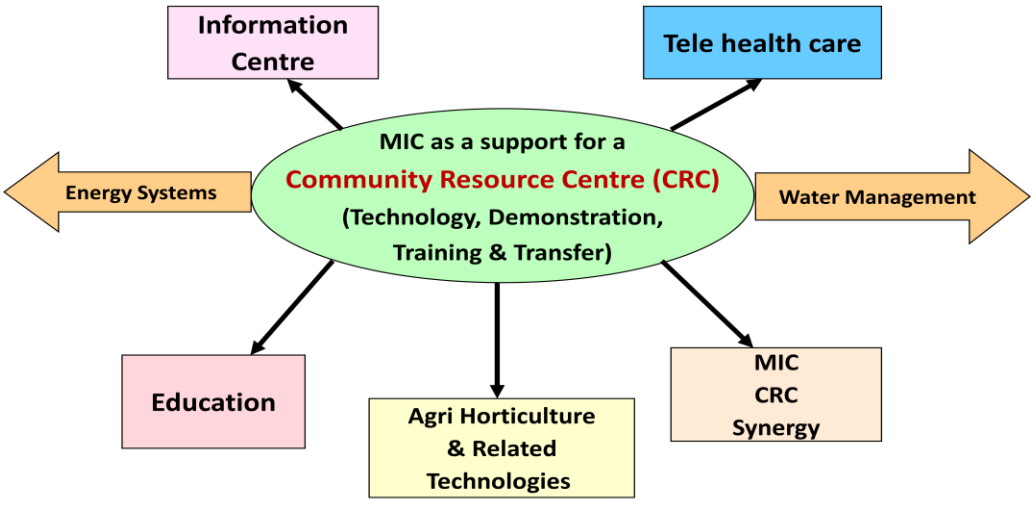

Fig. 9: Future Scenario: MIC as an anchor for Community Development

5. Conclusion

A MIC based on trigeneration has been designed and set-up in a rural hinterland. All the parameters which lead to sustainable development are incorporated in designing the system. It is envisaged that MIC can act as an anchor for development of the village cluster around it. The model could be replicated with appropriate technology mixes in other areas.

Acknowledgements

The authors are grateful for support through DST- RC-UK Science Bridge project (RP02260). Specifically we acknowledge DST for funding the Micro Industry at Malunga. Support given by Prof. Mohnot, The School of Desert Sciences, Jodhpur is gratefully acknowledged. The authors are thankful for the constant support and inputs from M/s IBL and M/s IB Turbo in implementing the work and for facilitating the project.

References

[1] P.K. Sen, Padma Vasudevan, S.N. Singh, Philip Davies, Sustainable Rural Micro Enterprises through Co and Tri generation: Review of concepts. J. Sci. & Ind. Res., 70, August (2011) 683-687.

[2] Padma Vasudevan, P.K. Sen, S.N. Singh, Prahlad Singh, Philip Davies, P.K. Dey, Robert Berry, Trigeneration using biomass energy for sustainable development, International Journal of Energy Sector Management, Vol. 7 (3), (2013) 309 – 320.

[3] A.K. Rajvanshi, V.Singh, N. Nimbkar, Biofuels-promise/prospects, paper presented at the conference at National Oilseeds Conference in Hyderabad, 29-31 January (2007), available at: www.nariphaltan.org/nari/pdf_files/ biofuels.pdf

[4] M. Tandon, P. Vasudevan, and S.N. Naik, Oil Bearing Seasonal Crops in India: Energy and Phytoremediation Potential, International Journal of Energy Sector Management, Vol. 7 (3), (2013) 338 – 354.

[5] I. Lewandowski, J.M.O. Scurlock, E. Lindvall, and M. Christou, The development and current status of perennial rhizomatous grasses as energy crops in the US and Europe, *Biomass and Bioenergy*, Vol. 25, (2003) 335-361.

[6] R.L.S. Lima, L.S. Severino, L.R. Sampaio, V. Sofiatti, J.A. Gomes and N.E.M. Beltrao, Blends of castor meal and castor husks for optimized use as organic fertilizer, Industrial Crops and Products, Vol. 33, (2011) 364-368.

[7] A.H. Grigoriou and G.A. Ntalos, The potential use of Ricinus communis L. (castor) stalks as a lignocellulosic resource for particleboards, Industrial Crops and Products, Vol. 13, (2001) 209-218.

[8] O.P. Toky, D.R. Black, P. Vasudevan and P.A. Davies, Biomass production in short rotation effluent-irrigated plantations in north-west India, J. Sci. & Ind. Res., Vol. 70, August (2011) 601-615.

[9] P. Vasudevan, A Thapliyal, R.K. Srivastava, A. Pandey, M.G. Dastidar and P. Davies, Fertigation potential of domestic wastewater for tree plantations, J. Sci. & Ind. Res., Vol. 69 (2010) 146-150.

[10] P. Vasudevan, P. Griffin, A. Warren, A. Thapliyal and M. Tandon, Localized domestic wastewater treatment: Part I – constructed wetlands (an overview). J. Sci. & Ind. Res., Vol. 70, No. 8 (2011) 583-594.

[11] P. Vasudevan, M. Tandon, P.K. Sen and S.N. Singh, Floating Wetlands: Comparison with Horizontal Flow Constructed Wetland, Int. J. Environmental Sciences, Vol. 1, No. 2 (2012) 159-171.

[12] P.K. Sen, P.V. Sen, A. Mudgal, S.N. Singh, S.K. Vyas and P. Davies, A small scale Multi-effect Distillation (MED) unit for rural micro enterprises: Part I-design and fabrication, Desalination, Vol. 279 (2011a) 15-26.

[13] P.K. Sen, P.V. Sen, A. Mudgal and S.N. Singh, A small scale Multi-effect Distillation (MED) unit for rural micro enterprises: Part II-Parametric studies and performance analysis, Desalination, Vol. 279 (2011b) 27-37.

[14] P.K. Sen, P.V. Sen, A. Mudgal and S.N. Singh, A small scale Multi-effect Distillation (MED) unit for rural micro enterprises: Part III- Heat transfer aspects, Desalination, Vol. 279 (2011c) 38-46.

[15] G.R. Desale, P. Vasudevan, J.K. Pothal, K.S. Zala, B.A. Bhatti, S.N. Singh, and P.K. Sen, Purification of water using vertical multi effect distillation unit, J. Sci. & Ind. Res., Vol. 70 (2011) 634-638.

[16] P.A. Davies, A.K. Hossain, Development of an integrated reverse osmosis – greenhouse system driven by solar photovoltaic generators, Desalination and Water Treatment, Vol. 22, No. 1-3 (2010) 161-173.